Supplementary Information

Lithium deposition mechanism on Si and Cu substrates in the carbonate electrolyte

Junhui Sun [a,b,#], Jiaying Peng[a,b,#], Terry Ring [c], Luisa Whittaker-Brooks [d], Juner Zhu [e], Dimitrios Fraggedakis [f], Jin Niu [a,b,*], Tao Gao [c,*], Feng Wang [a,b,*]

[a] State Key Laboratory of Chemical Resource Engineering, Beijing Key Laboratory of Electrochemical Process and Technology for Materials, Beijing University of Chemical Technology, Beijing 100029, P. R. China

[b] Beijing Advanced Innovation Center for Soft Matter Science and Engineering, Beijing University of Chemical Technology, Beijing 100029, P. R. China

[c] Department of Chemical Engineering, University of Utah, Salt Lake City, UT USA

[d] Department of Chemistry, University of Utah, Salt Lake City, UT USA

[e] Department of Mechanical Engineering, MIT, Cambridge, MA USA

[f] Department of Chemical Engineering, UC Berkeley, Berkeley, CA US

[#] These authors contributed equally

* Corresponding Authors.

E-mail: niujin@mail.buct.edu.cn; taogao@chemeng.utah.edu; wangf@mail.buct.edu.cn

Experiment

Preparation of Si thin film on copper foil

Si thin films were prepared via magnetron sputtering using n-type monocrystalline Si (purity 99.999%) and copper foil (thickness ~100 μm; area 0.1 × 0.1 m^2) as target and substrate, respectively. Prior to the deposition of Si, the copper foils were ultrasonic cleaned by acetone and ethanol to remove any surface impurities. The argon flow was adjusted to 40 sccm to achieve the desired working pressure of 0.01 mbar. The sputter processes were performed at 30 °C and the target was presputtered with Ar to remove impurities present on the target surface. Si thin films were deposited at a constant radio frequency (13.56 MHz) power supply of 250 W by controlling the deposition time.

Electrode Characterization

The morphology of electrode was characterized by scanning electron microscopy (SEM, JEOL, JSM-6701F) and atomic force microscope (AFM, DMFASTS-CAN2-SYS). The acceleration voltage for the SEM is 5 kV. After Li electrodeposition onto electrode, the cells were immediately disassembled in the argon-filled glove box (MIKROUNA, Universal) and the electrodes were rinsed with fresh dimethyl carbonate (DMC) and dried. The washed Electrodes were mounted onto SEM stages and sealed in Ar-filled transfer vessels for immediate SEM observation. The cross-sections were cut by applying a cross-section polisher (JEOL, IB-19530CP). Raman spectra of the Si film were obtained using a LabRam HR800 spectrometer. The surface chemical compositions of the Si film were analyzed by X-ray photoelectron spectroscopy (XPS, ESCALAB 250). *In-situ* optical microscopy analyses were conducted on an optical microscope (XJ-550) with an electrolytic cell (Beijing Scistar Technology Co. Ltd). Cu foil with Si film, separator, lithium foil, and glass plate were assembled together in the Ar-filled glove box according to the schematic (Figure S1). 1.0 M solution of $LiPF_6$ in ethylene carbonate (EC), diethyl carbonate (DEC), and DMC (1:1:1 by vol.) with 5 wt.% fluoroethylene carbonate (FEC) was used as the electrolyte and added into the cell. Lithium foil and separator were punched at the center for the deposit observation.

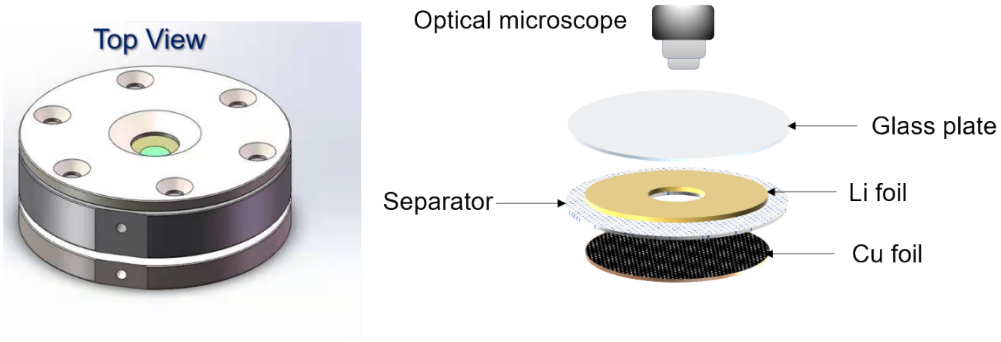

Supporting Figure S1. Schematic of the *in-situ* optical cell.

Electrochemical testing

2032-type coin cells with working electrodes and Li foil (China Energy Lithium, ϕ 15 × 0.5 mm) counter electrodes were assembled in the argon-filled glove box. The electrolyte was 1.0 M solution of $LiPF_6$ in ethylene carbonate (EC), diethyl carbonate (DEC), and DMC (1:1:1 by vol.) with 5 wt.% fluoroethylene carbonate (FEC) and 100 μL electrolyte was added to each cell. The separator was polypropylene membrane (Celgard 2400). The coin cells were sealed using a Hydraulic Crimping machine at approximately 5 MPa (MTI Corporation, MSK-110).

Galvanostatic tests were carried out using a Land CT2001A system. For the Li lithiation/delithiation cycling, the cells were galvanostatically charged-discharged from 0.01 to 1V (*vs.* Li^+/Li). The Li deposition capacity is determined from the nucleation formation. For the Li deposition/stripping cycling, the cells were discharged at 0.1, 1, 10 mA cm^{-2} to 0.5, 1 mAh cm^{-2}, followed by being charged to 0.5 V (*vs.* Li^+/Li). Since the initial CE of the Si film is low, this should be taken into account in evaluation the of Li deposition reversibility. Therefore, the average CE was obtained from 3^{th} to 100^{th} cycle. All temperature-related electrochemical measurements were conducted in a temperature and humidity testing chamber (POOSANDA, BY-260TH). For the EIS measurements, the frequency was in the range of 100 kHz to 100 mHz.

Imaging and analysis

The size of deposited Li, including area, perimeter and the diameter of whisker (the ratio of length to width of deposited Li is more than 5:1), were measured using ImageJ software. Nuclei density was measured using Nano Measurer software by dividing the

number of visible particles by the area of the corresponding view field. At least 5 randomly selected images were averaged for each test condition.

For the fitting analysis, the error bars indicate the standard deviation of multiple data, and the iterative algorithm of orthogonal distance regression is adopted considering the error bars.

Molecular dynamics simulation of Li deposition

Molecular dynamics simulations were performed using the Large-scale Atomic/Molecular Massively Parallel Simulator (LAMMPS)[1]. The atomic scale trajectory information was visualized by using the Open Visualization Tool (Ovito)[2].

MD simulation were used to study the temporal evolution of Li deposition on a Cu and $Li_{15}Si_4$ surface at 0 kPa with periodic boundary conditions and all the simulation are perform at 300K with a time step of 1ns and a cutoff distance of 10 Å. The Cu and $Li_{15}Si_4$ substrates used in the simulations comprised 19600 and 15264 atoms arranged in a face-centred cubic lattice structure and the cubic $I\bar{4}3d$ space group with a domain of 12.65nm (length) × 12.65 nm (width) × 1.45 nm (height).

An initial energy minimization of the Cu and $Li_{15}Si_4$ surface was performed with 0 and 10-8 eV $Å^{-1}$ energy and force cutoff, respectively. The Li deposition was directed to the Cu and $Li_{15}Si_4$ surface with a total area of 150 nm^2 over 1 ns at a deposition rate of 5 Li ps^{-1}. The Li deposition was simulated in an isothermal-isobaric ensemble (NPT) with a Nose-Hoover thermostat and barostat[3].

The Li-Li and Cu-Cu atomic interactions were simulated with the MEAM potentials[4], Si-Si atomic interactions were simulated with the Tersoff potentials[5]. whereas the Li-Cu and Li-Si interactions were modelled with the Lennard-Jones 6-12 interatomic potentials with the following Lennard-Jones potential parameters obtained by the Lorentz-Berthelot arithmetic mixing rules: $\varepsilon_{Cu\text{-}Li}$ = 0.047 eV and $\sigma_{Cu\text{-}Li}$ = 2.182 Å[6]. And $\varepsilon_{Li\text{-}Si}$ = 0.015 eV and $\sigma_{Li\text{-}Si}$ = 3.173 Å from the available Lennard-Jones potential parameters for the pure Li[7], Si[8] atoms.

Supplementary figures, tables and related discussion

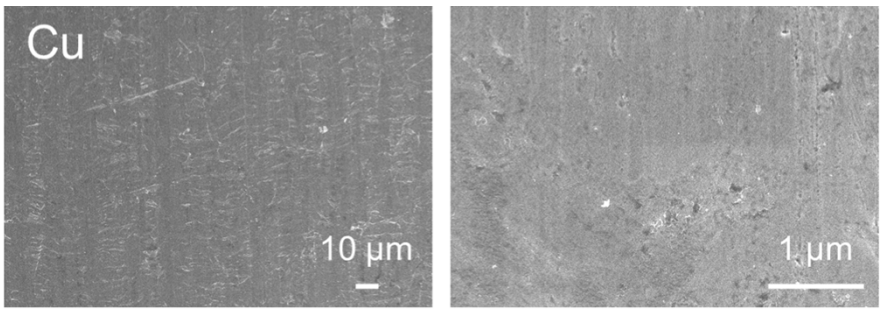

Supporting Figure S2. SEM images of Cu foil.

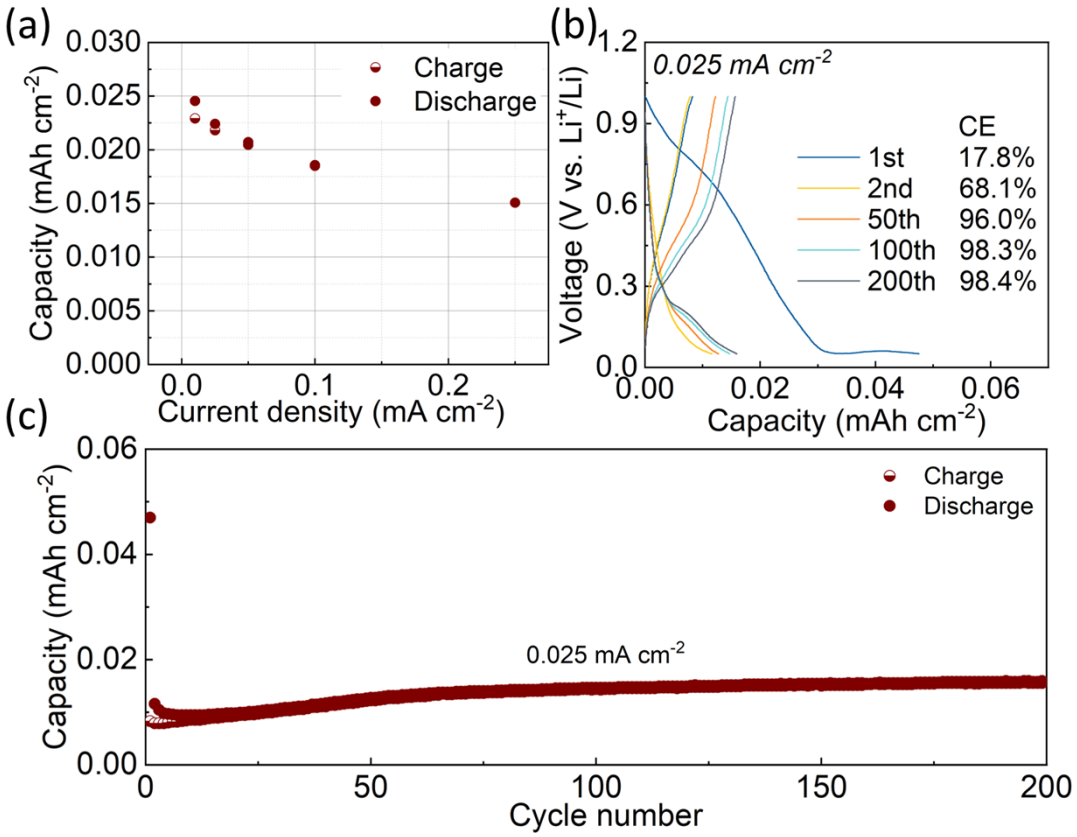

Supporting Figure S3. The electrochemical properties of the silicon film.

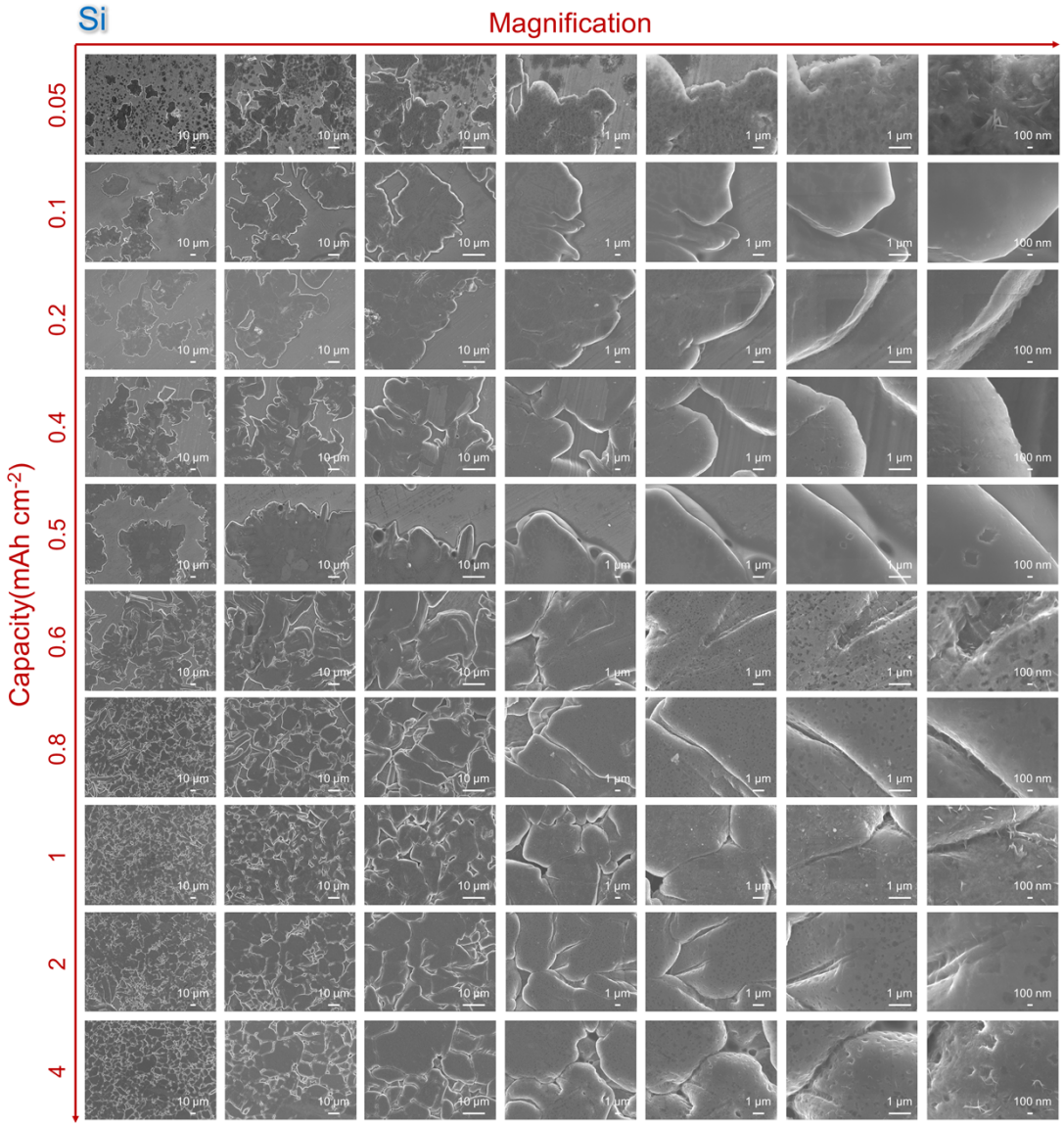

Supporting Figure S4. Li growth on Si. SEM images of Li deposits at different capacities, J=0.025 mA cm^{-2}.

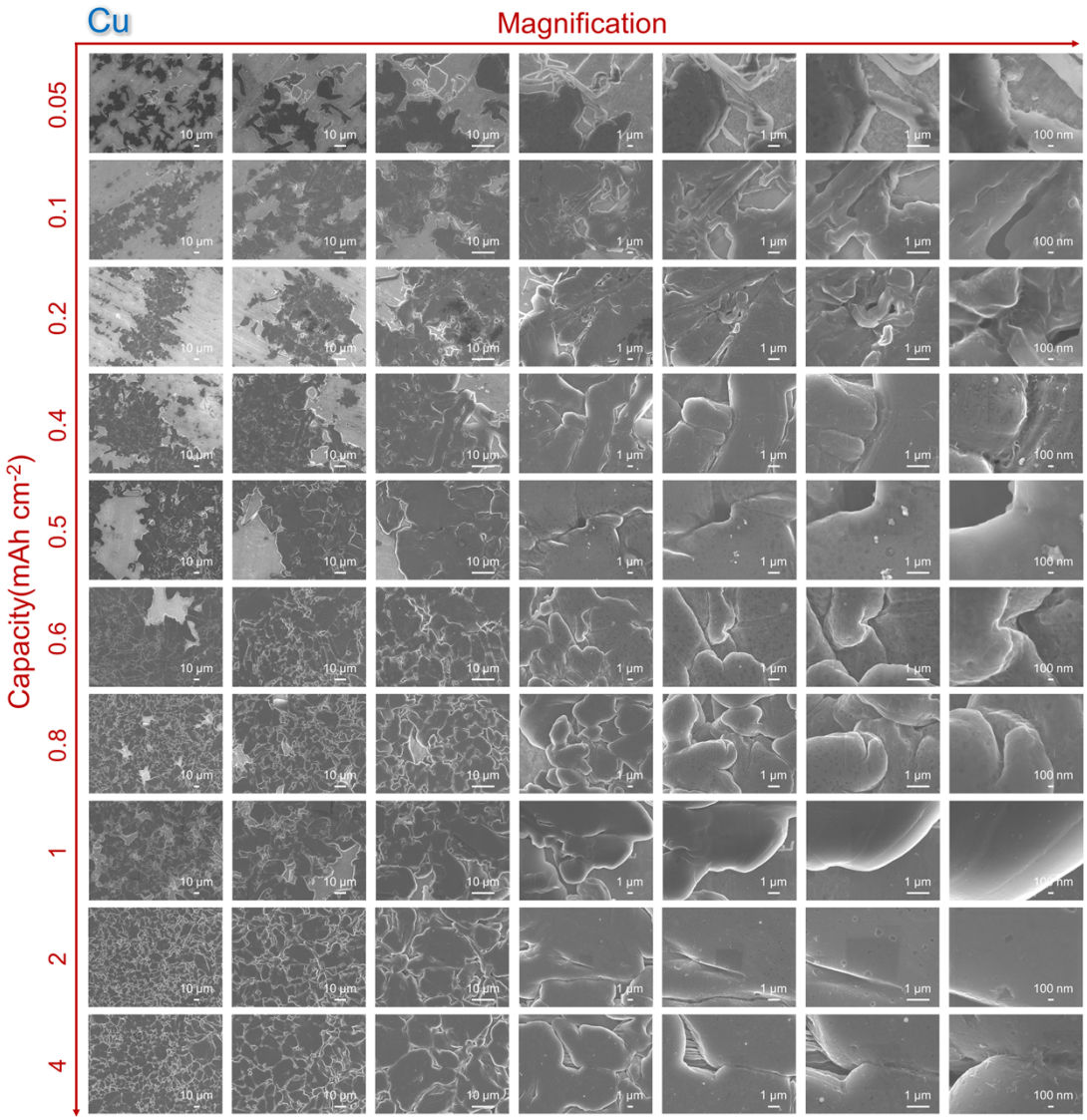

Supporting Figure S5. Li growth on Cu. SEM images of Li deposits at different capacities, J=0.025 mA cm^{-2}.

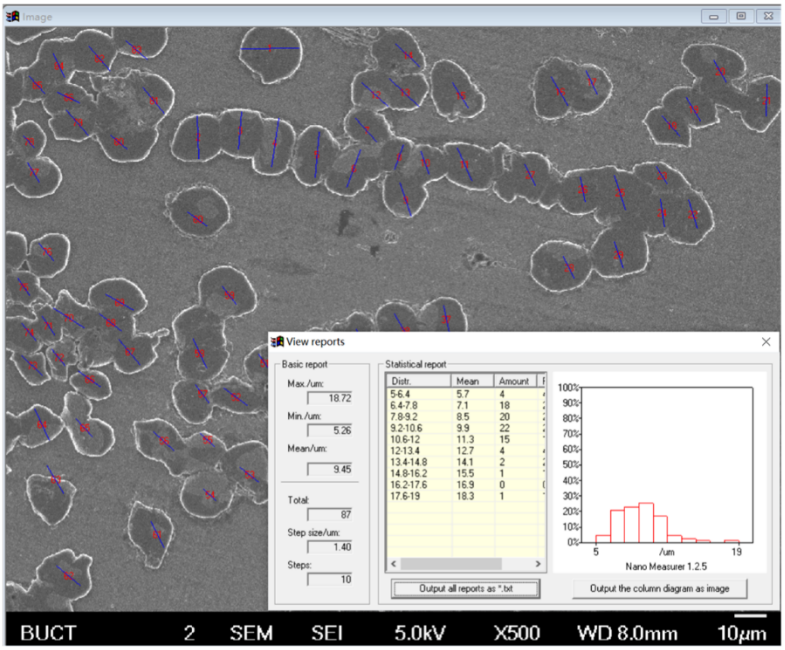

Supporting Figure S6. The number and size of the individual deposits using Nano Measurer.

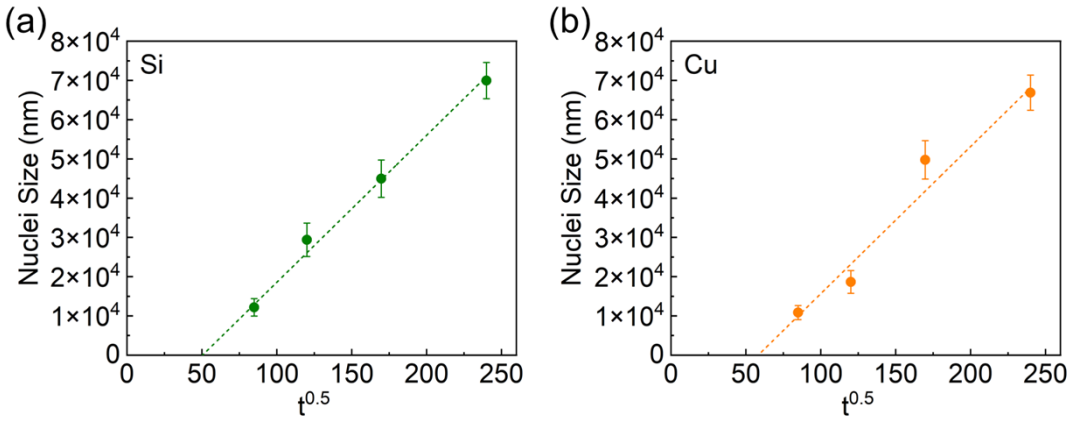

Supporting Figure S7. Li growth at 0.025 mA cm^{-2} with one spacer in the coin cell.

Fitting curve: $y = ax + b$

Si: a= 22.47; b= -18.9; R^2= 0.992;

Cu: a= 22.47; b= -21.79 ; R^2= 0.953

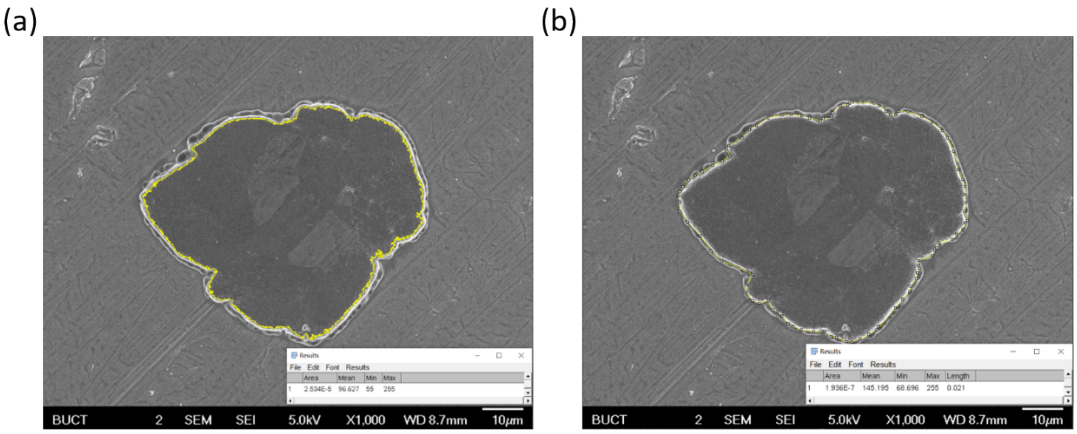

Supporting Figure S8. Area and perimeter calculation using ImageJ.

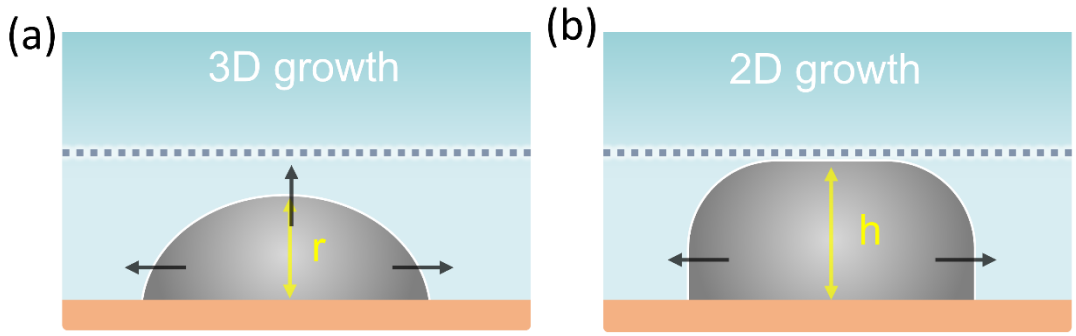

Supporting Figure S9. Schematic of 3D and 2D growth.

3D growth:

$$Q = {}^{2}/_{3}\pi r^{3}\rho C_{s}N, r = \left(\frac{3}{2\pi\rho C_{s}N}\right)^{1/3}Q^{1/3}$$

$$\varphi = \pi r^{2}N$$

$$\frac{\varphi}{Q} = \frac{3}{2\rho C_{s}r}\frac{1}{}$$

$$\varphi = \frac{3}{2\rho C_{s}r}\frac{1}{}Q$$

$$\varphi = k_{1}Q^{2/3}, k_{1} = 0.0118\ N^{1/3}$$ (Supporting Equation 1)

where Q is Li deposition capacity, φ is area coverage, ρ is the density of Li metal (0.534 g cm^{-3}), C_s is theoretical specific capacity of Li metal (3860 mAh g^{-1}), N is the nucleation density.

2D growth:

$$Q = S_{dep}h\rho C_{s}N$$

$$\varphi = S_{dep}N$$

$$\frac{\varphi}{Q} = \frac{1}{\rho C_{s}h}\frac{1}{}$$

$$\varphi = \frac{1}{\rho C_{s}h}\frac{1}{}Q$$

$$\varphi = k_{2}Q, k_{2} = 4.85 \times 10^{-4}\frac{1}{h}$$ (Supporting Equation 2)

where S_{dep} is the area of single Li deposit , h is the thickness of Li deposit, A is the area of substrate.

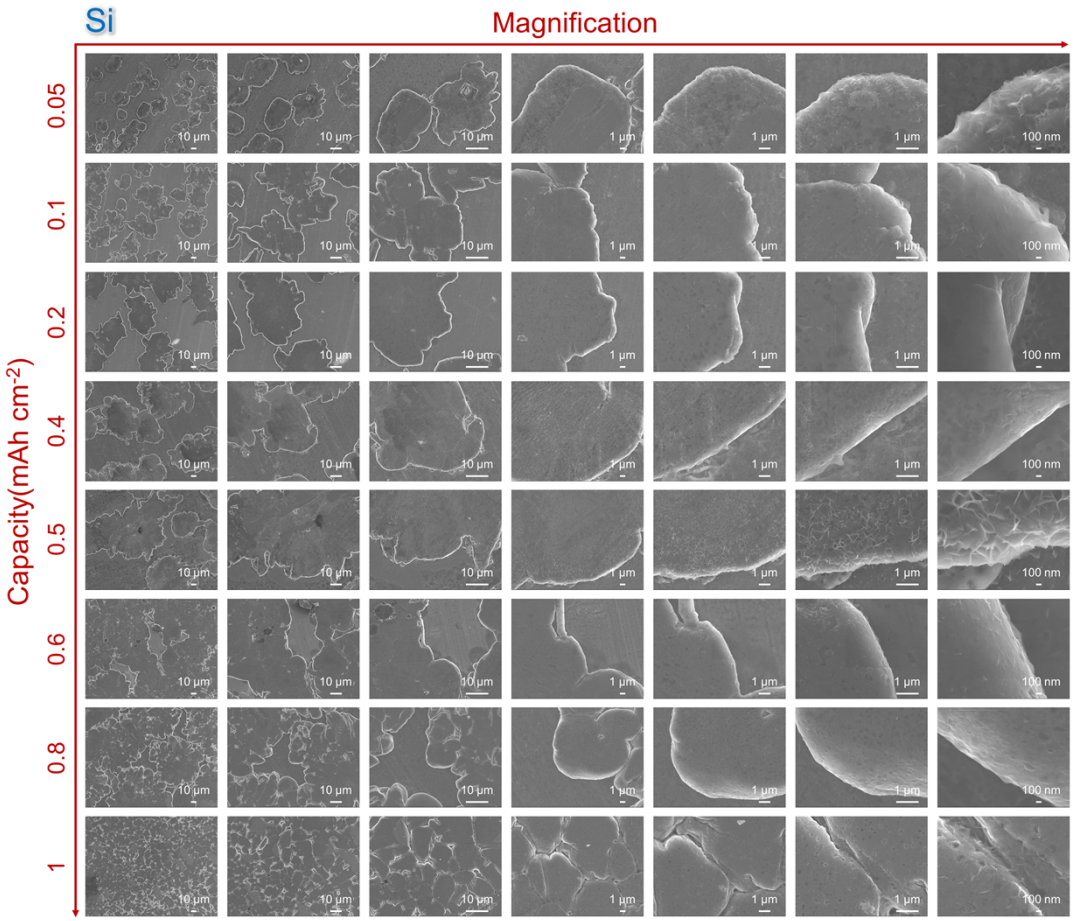

Supporting Figure S10. Li growth on Si. SEM images of Li deposits at different capacities with two spacers in the coin cell, J=0.025 mA cm^{-2}.

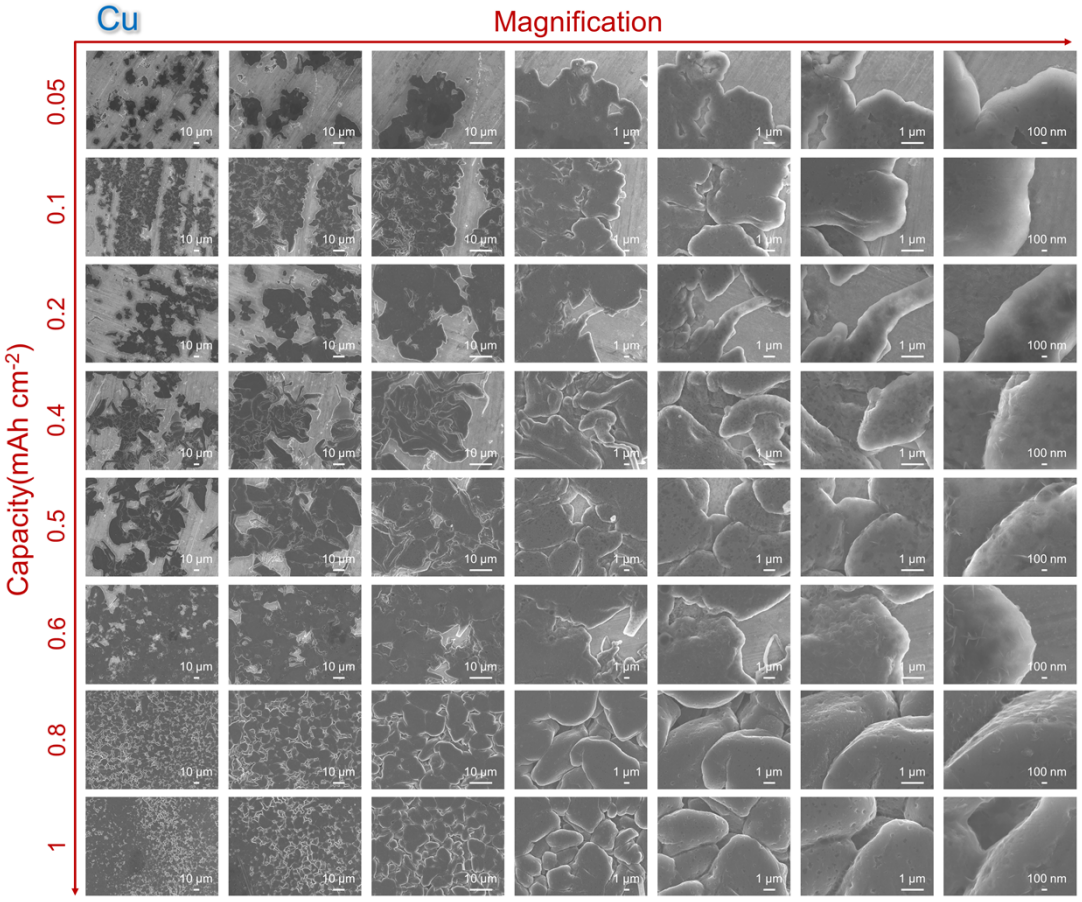

Supporting Figure S11. Li growth on Si. SEM images of Li deposits at different capacities with two spacers in the coin cell, J=0.025 mA cm^{-2}.

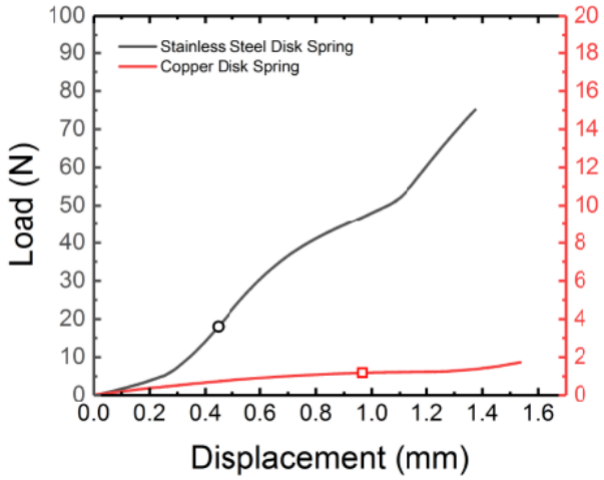

Supporting Figure S12. Nonlinear force-displacement response of compressing stainless steel disk spring and copper disk spring.

Figure S12 shows the nonlinear force-displacement response of compressing stainless steel disk spring and copper disk spring. The stainless steel one has higher stiffness and the copper one has lower. In our paper, we used the stainless steel one. In the single-spacer case, the thickness change after assembling/crimping is 0.075 mm (before: 3.235 mm, after: 3.160 mm). According to the nonlinear force-displacement response in the figure below, this amount of displacement results in a force of 1.25 N. Because the plate is 7 mm in radius, the stress on the Li foil is 8.12 kPa. In the double-spacer case, the thickness change is 0.755 mm (before: 4.235 mm, after: 3.480 mm). This amount of displacement results in a force of 39 N, which is 253.2 kPa.

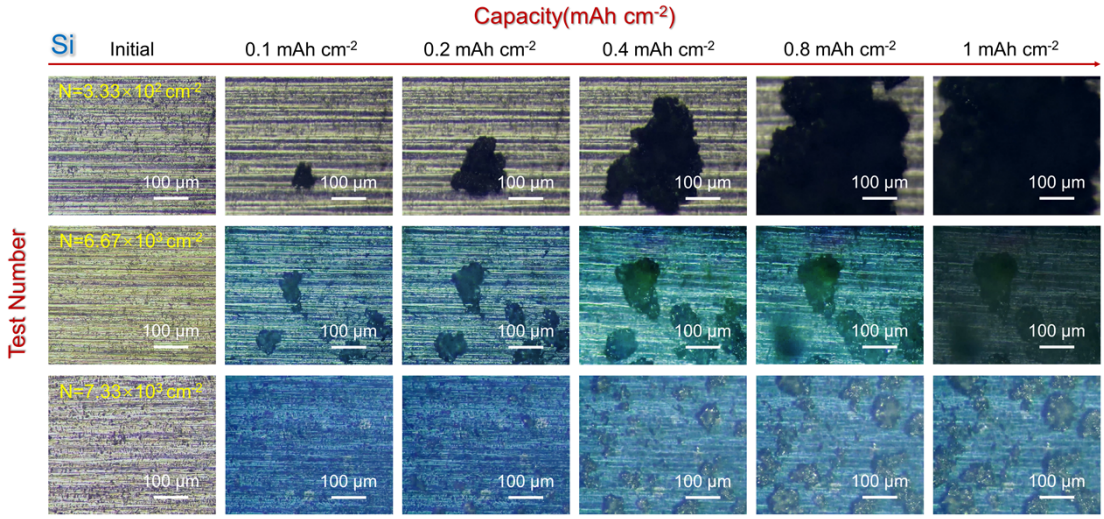

Supporting Figure S13. In-situ optical test of Si thin film.

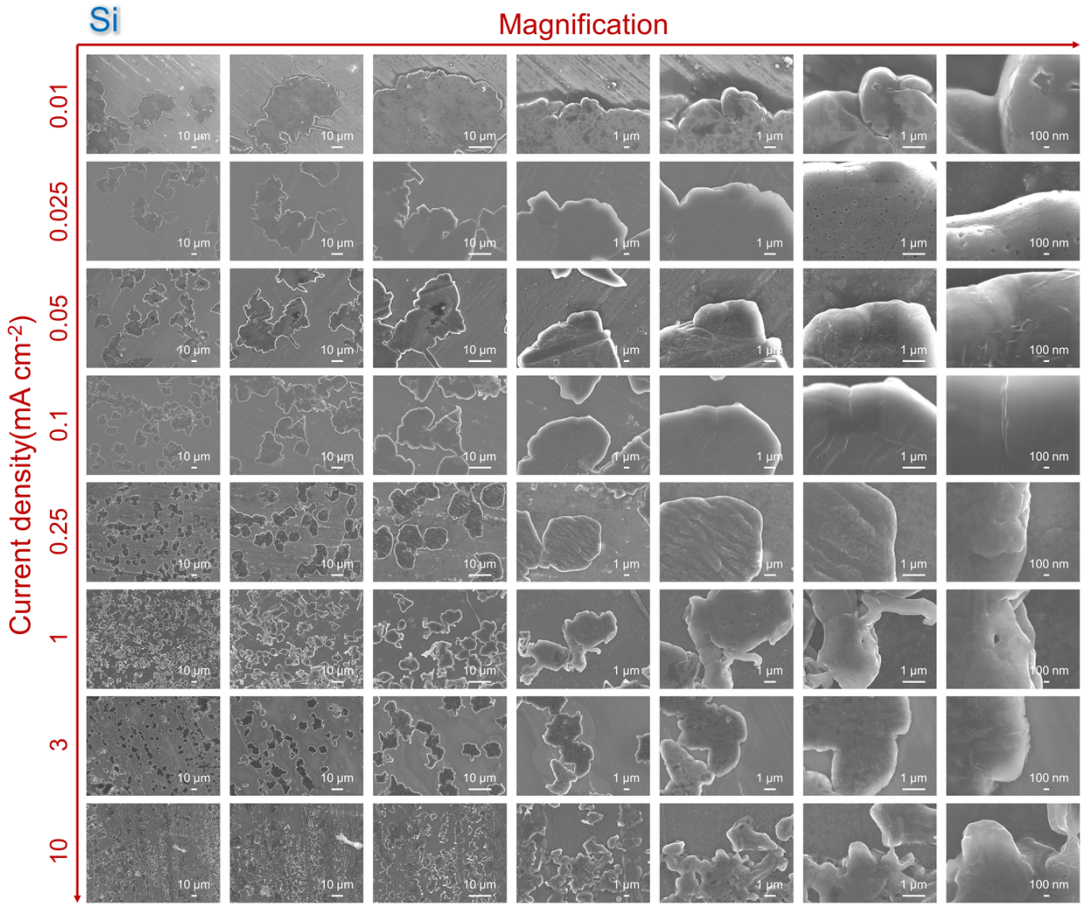

Supporting Figure S14. Li growth on Si. SEM images of Li deposits at different current densities, Q=0.1 mAh cm^{-2}.

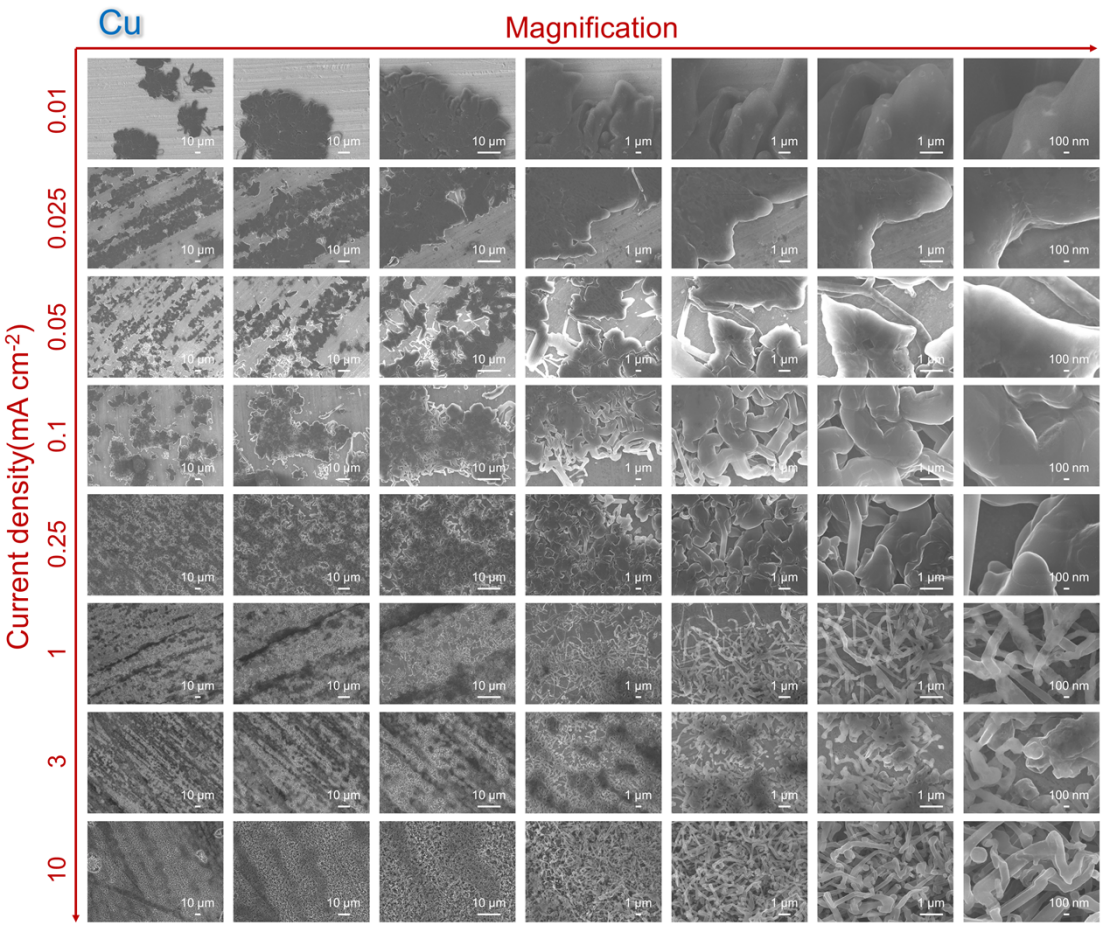

Supporting Figure S15. Li growth on Cu. SEM images of Li deposits at different current densities, Q=0.1 mAh cm^{-2}.

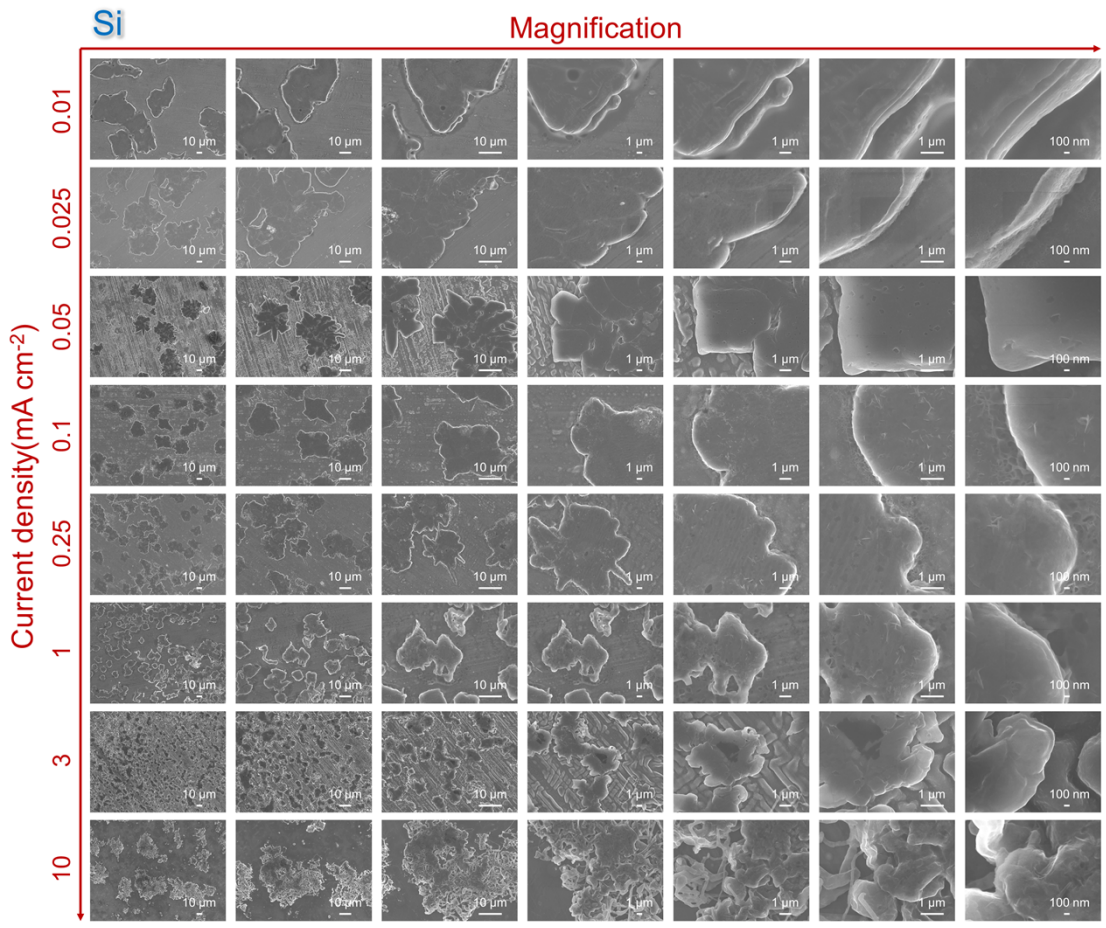

Supporting Figure S16. Li growth on Si. SEM images of Li deposits at different current densities, Q=0.2 mAh cm^{-2}.

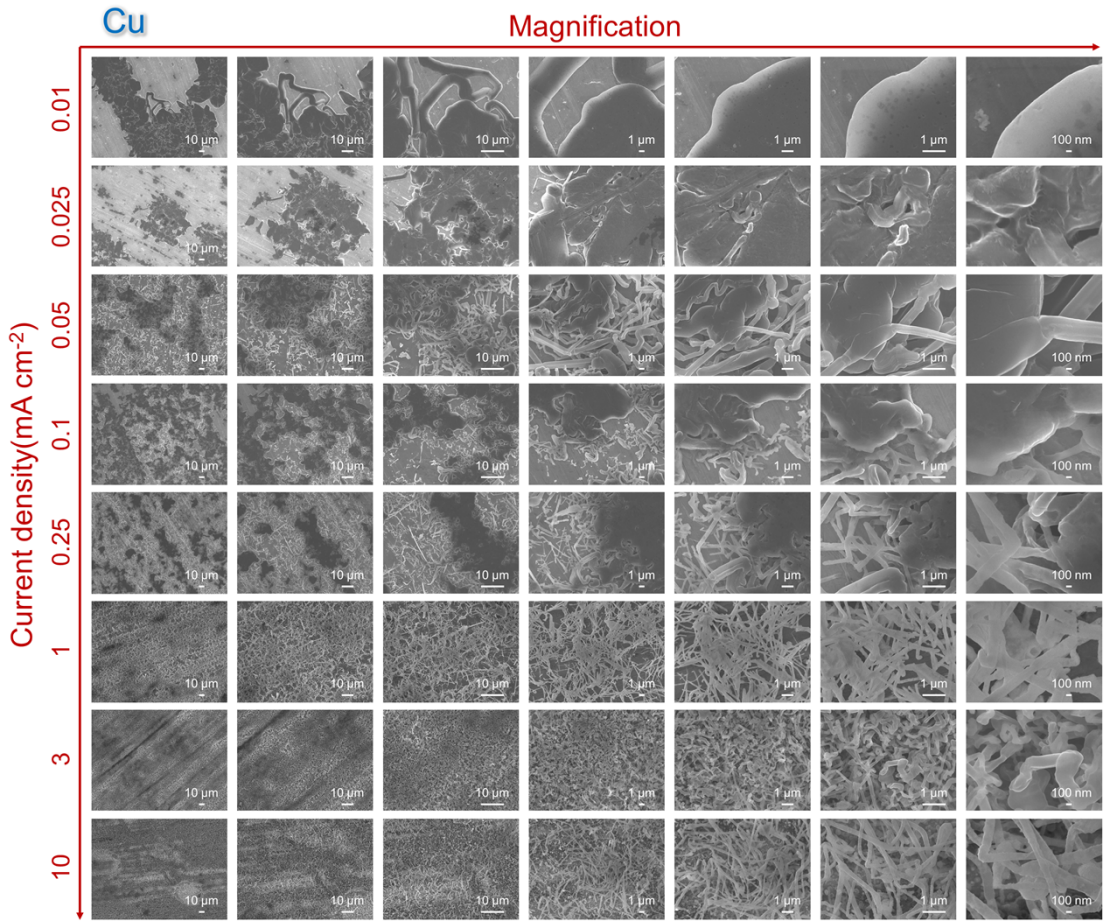

Supporting Figure S17. Li growth on Cu. SEM images of Li deposits at different current densities, Q=0.2 mAh cm^{-2}.

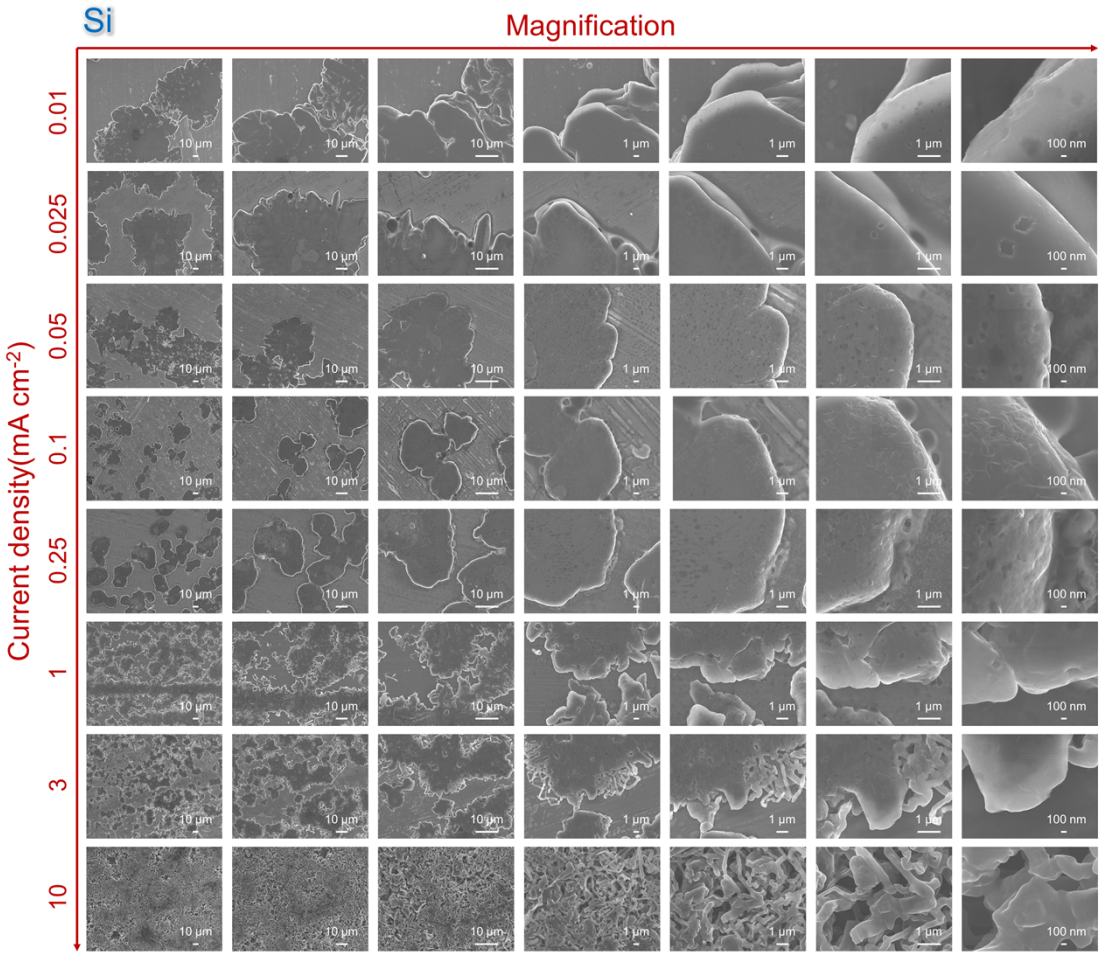

Supporting Figure S18. Li growth on Si. SEM images of Li deposits at different current densities, Q=0.5 mAh cm^{-2}.

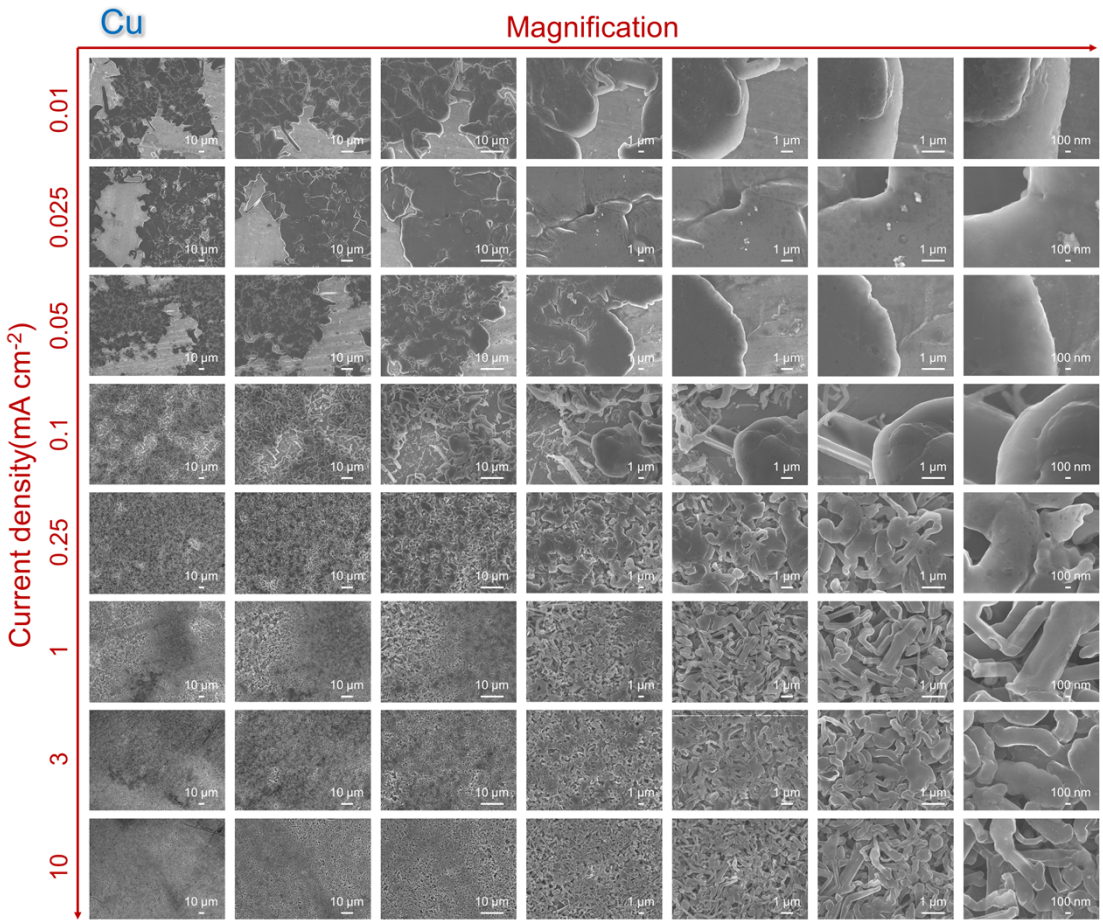

Supporting Figure S19. Li growth on Cu. SEM images of Li deposits at different current densities, Q=0.5 mAh cm^{-2}.

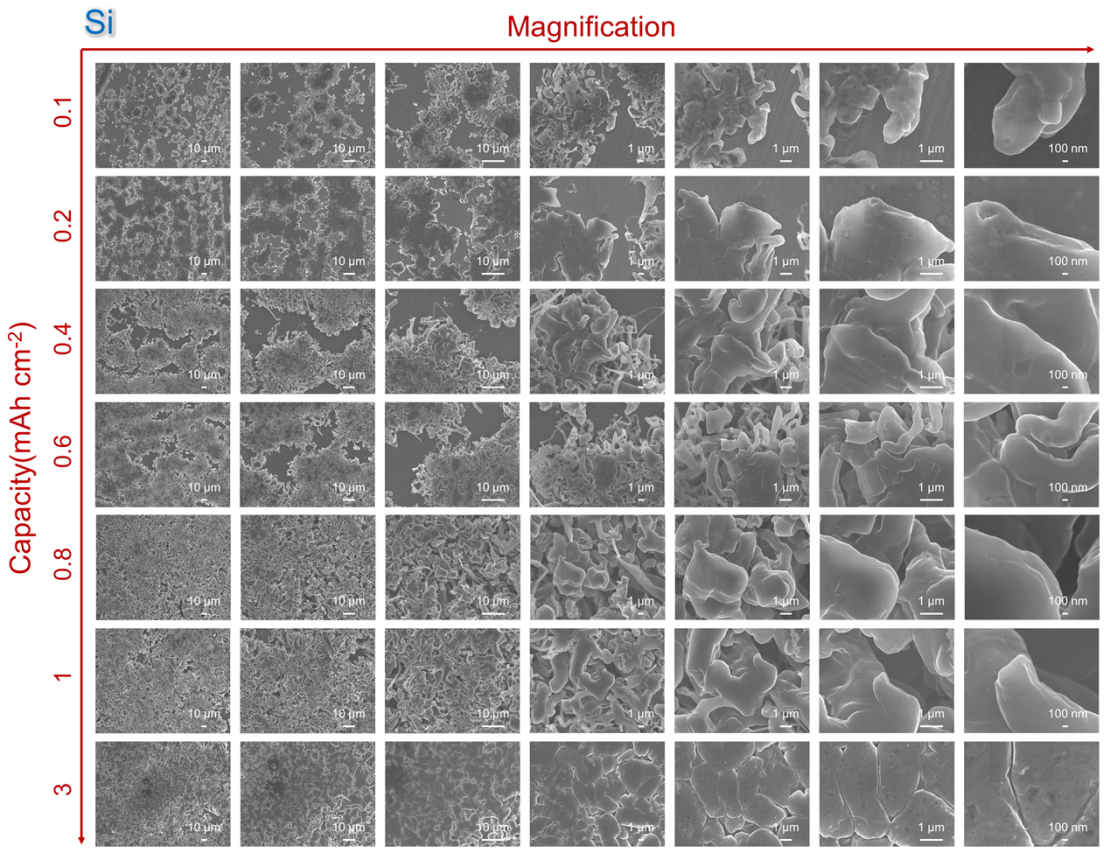

Supporting Figure S20. Li growth on Si. SEM images of Li deposits at different capacities, J=1 mA cm^{-2}.

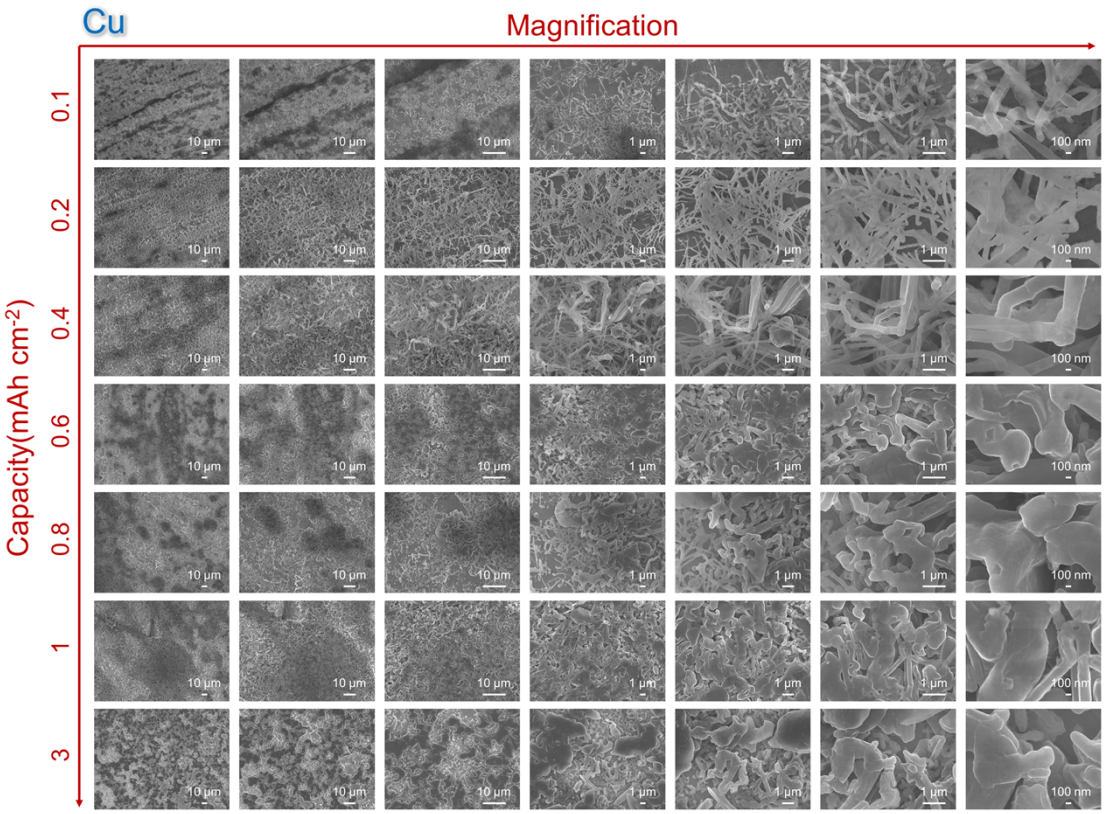

Supporting Figure S21. Li growth on Cu. SEM images of Li deposits at different capacities, J=1 mA cm^{-2}.

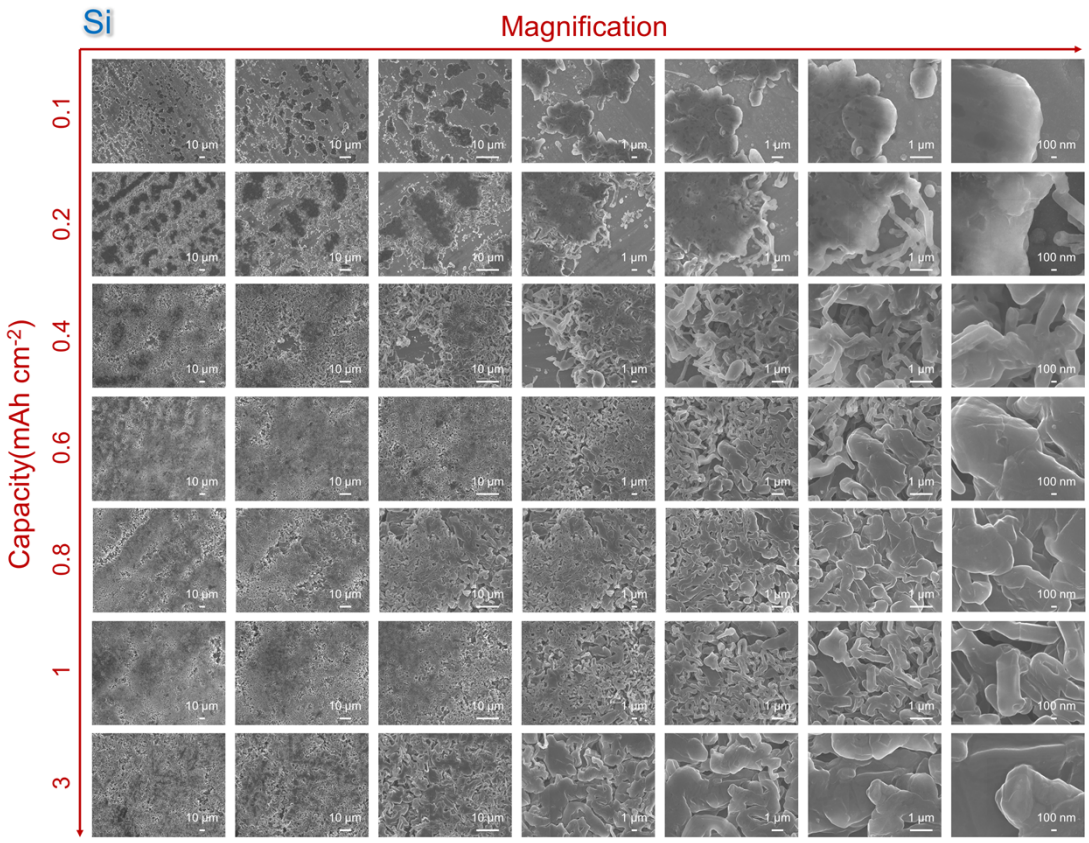

Supporting Figure S22. Li growth on Si. SEM images of Li deposits at different capacities, J=10 mA cm^{-2}.

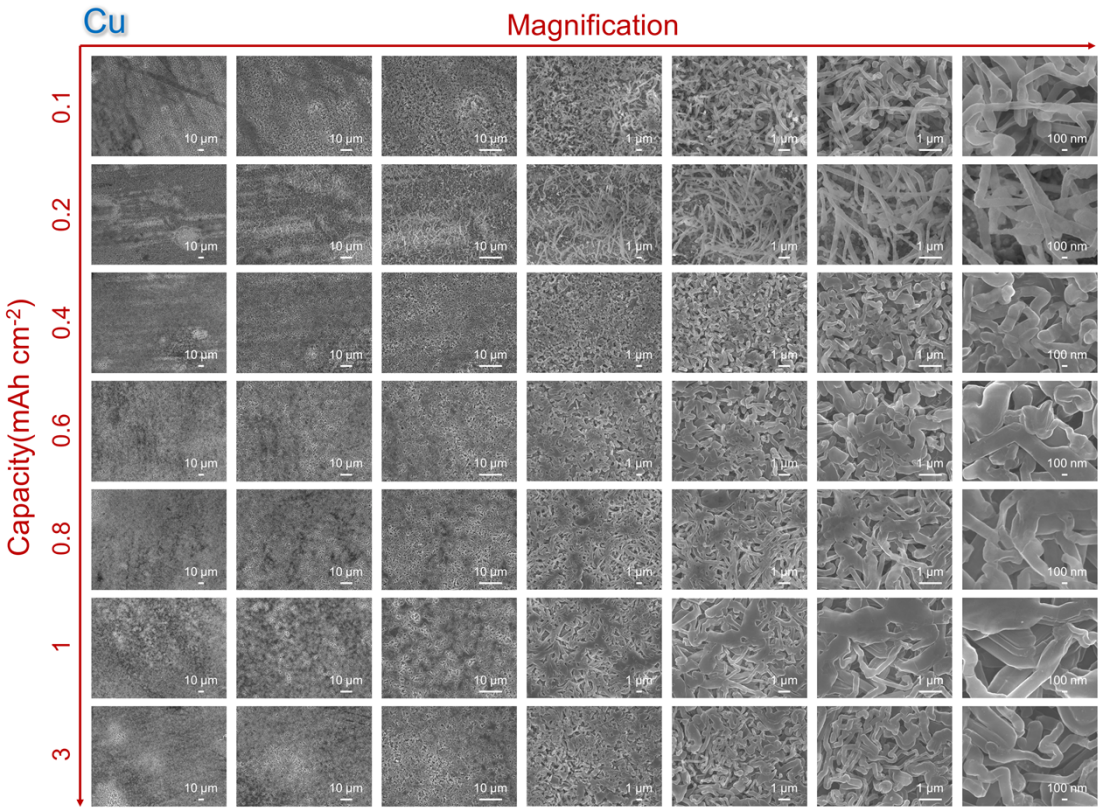

Supporting Figure S23. Li growth on Cu. SEM images of Li deposits at different capacities, J=10 mA cm^{-2}.

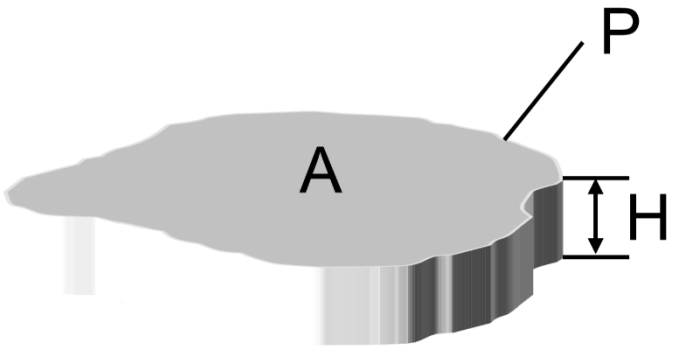

Supporting Figure S24. Schematic of 2D Li deposit.

$$R_{SA/V} = \frac{SA}{V} = \frac{A + PH}{AH} = \frac{1}{H} + \frac{P}{A}$$ (Supporting Equation 3)

where SA is the surface area of 2D Li deposit, V is the volume of 2D Li deposit, A is the area of 2D Li deposit , P is the perimeter of 2D Li deposit, H is the thickness of Li deposit.

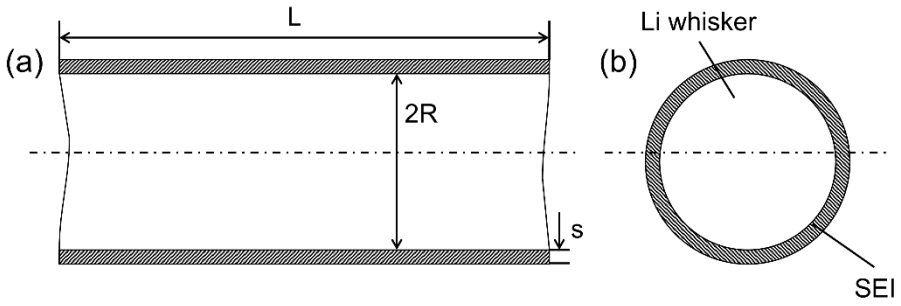

Supporting Figure S25. Schematic diagram of longitudinal (a) and transverse (b) sections of Li whisker.

$V_{Li} = \pi R^2 L$

$dV_{Li} = 2\pi RLdR$

$V_{SEI} = \pi(R+s)^2 L - \pi R^2 L = \pi L(s^2 + 2Rs) \approx 2\pi LRs$, since $\frac{s}{R} \ll 1$

$dV_{SEI} = 2\pi L(Rds + sdR)$, Rds due to thickness increase; sdR due to area increase.

Theory:

$Q_1 = \frac{dn_{Li}}{dt} = \frac{d(c_{Li}V_{Li})}{dt} = c_{Li}\frac{dV_{Li}}{dt} = c_{Li}\cdot 2\pi RL\cdot\frac{dR}{dt}$, c_{Li} is Li concentration in Li metal.

Total Li^+ flux contributing to Li growth

$Q_2 = \psi\cdot A = J\cdot 2\pi RL = D_{Li^+}^{SEI}\frac{c_0}{s}\cdot 2\pi RL$, c_0 is Li concentration in electrolyte.

Diffusion-limited growth means:

$Q_1 = Q_2$

$\frac{dn_{Li}}{dt} = \psi\cdot A$

$c_{Li}\cdot 2\pi RL\cdot\frac{dR}{dt} = D_{Li^+}^{SEI}\frac{c_0}{s}\cdot 2\pi RL$

$dR = \frac{c_0}{c_{Li}}D_{Li^+}^{SEI}\frac{dt}{s}$, let $\beta = \frac{c_0}{c_{Li}}D_{Li^+}^{SEI}$,

$dR = \beta\frac{dt}{s}$, β is constant. (Supporting Equation 4)

If s is a constant, then $R \sim \frac{\beta}{s} t$, which does not agree with experiment.

Experiment finds $R \sim t^{1/2}$

So $dR \sim \frac{1}{2} \frac{dt}{t^{1/2}}$ (Supporting Equation 5)

Compare (Equation S4) with (Equation S5),

$s \sim t^{1/2}$

Therefore, the growth of SEI is also diffusion-limited. In this case, it is limited by diffusion of solvent through SEI

In electrolyte, solvent is reduced to SEI at 1.0 V vs. Li^+/Li. Li^+ is reduced to Li metal at 0 V vs. Li^+/Li.

Depending on how fast Li deposit grows and how well SEI can accommodate the strain, there are three modes SEI can grow.

(1) Li deposit grows very fast so that SEI cracks then new SEI forms at the gap right away. (Fig. S25-1, if tensile stress is greater than SEI's yield stress)

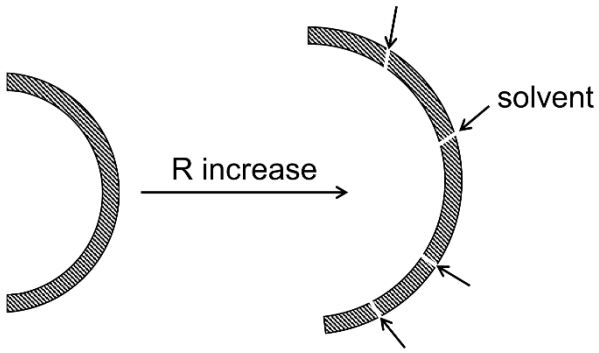

Supporting Figure S25-1. SEI growth mode I

(2) Li deposit grows slowly, so that SEI is stretched and thinned like a balloon, which decreases the diffusion length of solvent and increase the diffusion flux. The reduced solvent add new materials to SEI and thickens it until new equilibrium is established. (Fig. S25-2)

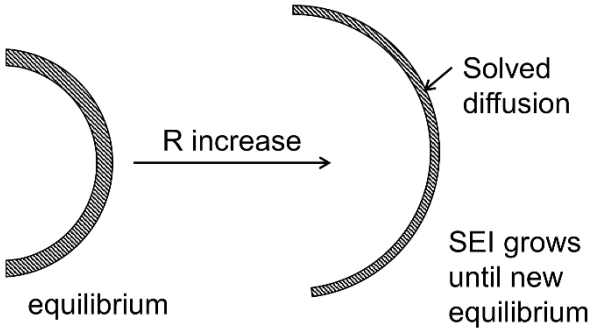

Supporting Figure S25-2. SEI growth mode II

$c_{SEI}\frac{ds}{dt} = \psi_{Solvent} = D_{Sol}^{SEI}\frac{c_{Sol}}{s}$, c_{SEI} is equilibrium concentration of solvent in SEI.

For uniform deposition so that R does not change.

$$c_{SEI}(s\frac{dR}{dt} + R\frac{ds}{dt}) = \psi_{Solvent} = D_{Sol}^{SEI}\frac{c_{Sol}}{s}R$$

For a cylinder deposit grows only in radial direction. (whisker)

(3) SEI growth due to leaking of electrons.

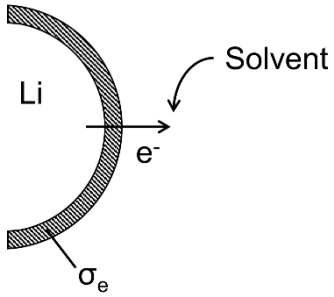

Supporting Figure S25-3. SEI growth mode III

$$c_{SEI}\frac{ds}{dt} \sim I_{SEI} \sim \frac{\Delta V}{\frac{1}{\sigma_e}s}$$

$\frac{ds}{dt} \sim \frac{\sigma_e\ \Delta V}{c_{SEI}\ s}$ Driving force for SEI reduction const for a given solvent.

$$sds \sim \frac{\sigma_e}{c_{SEI}}\Delta V dt$$

$$s^2 \sim \frac{\sigma_e}{c_{SEI}} \Delta V t$$

$$s \sim t^{1/2}$$

Compare Mode II with Mode III.

Mode II: $\frac{ds}{dt} = \frac{D_{Sol}^{SEI}}{c_{SEI}} c_{Sol} \frac{1}{s}$

Mode III: $\frac{ds}{dt} \sim \frac{\sigma_e}{c_{SEI}} \Delta V \frac{1}{s}$

Growth speed ratio: $\frac{\text{II}}{\text{III}} = \frac{D_{Sol}^{SEI} c_{Sol}}{\sigma_e \Delta V}$, depending on speed of solvent diffusion and e^- leaking.

Initial formation and growth of SEI

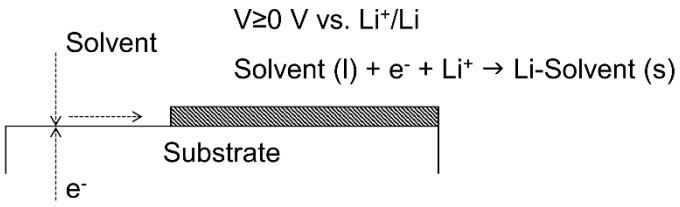

Assuming reaction-controlled until reach certain thickness

$$\psi = k_0 c_{sol} f(\eta) = c_{SEI} \frac{ds}{dt}$$

$$ds = \frac{k_0 c_{sol}}{c_{SEI}} f(\eta) dt$$ $k_0 c_{sol}$ is constant.

Assuming const η, $s = k_0 \frac{c_{sol}}{c_{SEI}} f(\eta) t$ (Linear growth), until s becomes very thick so diffusion is the limiting factor.

Solve $c_{SEI} \frac{ds}{dt} = \psi_{Sol} = D_{Sol}^{SEI} \frac{c_{Sol}}{s}$

$$s ds = \frac{c_{Sol}}{c_{SEI}} D_{Sol}^{SEI} dt$$

$$\frac{1}{2} s^2 = \frac{c_{Sol}}{c_{SEI}} D_{Sol}^{SEI} t + const_1$$

Initial condition: $s_{t=0} = 0$, $const_1 = 0$

$$\frac{1}{2}s^2 = \frac{c_{Sol}}{c_{SEI}} D_{Sol}^{SEI} t$$

$$s = \left(\frac{2c_{Sol}}{c_{SEI}} D_{Sol}^{SEI}\right)^{1/2} t^{1/2} \quad \text{let} \quad \alpha = \frac{c_{Sol}}{c_{SEI}} D_{Sol}^{SEI}$$

$s = (2\alpha)^{1/2} t^{1/2}$ gives SEI thickness as a function of time (Supporting Equation 6)

Since $dR = \beta \frac{dt}{s}$, $\beta = \frac{c_0}{c_{Li}} D_{Li^+}^{SEI}$, plug in (Equation S6)

$$dR = \beta (2\alpha)^{-1/2} t^{-1/2} dt = \beta \left(\frac{2}{\alpha}\right)^{\frac{1}{2}} d(t^{1/2})$$

$$R = \beta \left(\frac{2}{\alpha}\right)^{\frac{1}{2}} t^{1/2} + const_2$$

Initial condition: $R_{t=0} = 0$, $const_2 = 0$

$$R = \beta \left(\frac{2}{\alpha}\right)^{\frac{1}{2}} t^{1/2} = 1.41 \frac{\beta}{\sqrt{\alpha}} t^{1/2}, \quad \beta = \frac{c_0}{c_{Li}} D_{Li^+}^{SEI}, \quad \alpha = \frac{c_{Sol}}{c_{SEI}} D_{Sol}^{SEI}$$

$c_0 = 1\ mol/L$

$$c_{Li} = \frac{n_{Li}}{V_{Li}} = \frac{\rho}{M} = \frac{0.534\ g/cm^3}{7\ g/mol} = 76.3\ mol/L$$

For pure EC, $c_{Sol} = \frac{n_{Sol}}{V_{Sol}} = \frac{\rho}{M} = \frac{1.32\ g/cm^3}{88.06\ g/mol} = 14.99\ mol/L$ (31.67%)

For pure DMC, $c_{Sol} = \frac{n_{Sol}}{V_{Sol}} = \frac{\rho}{M} = \frac{1.07\ g/cm^3}{90.08\ g/mol} = 11.88\ mol/L$ (31.67%)

For pure DEC, $c_{Sol} = \frac{n_{Sol}}{V_{Sol}} = \frac{\rho}{M} = \frac{0.98\ g/cm^3}{118.13\ g/mol} = 8.30\ mol/L$ (31.67%)

For pure FEC, $c_{Sol} = \frac{n_{Sol}}{V_{Sol}} = \frac{\rho}{M} = \frac{1.45\ g/cm^3}{106.05\ g/mol} = 13.67\ mol/L$ (5%)

$c_{Sol} = 11.82\ mol/L$

For Li_2CO_3, $c_{SEI} = 2 \times \frac{\rho}{M} = 2 \times \frac{2.11\ g/cm^3}{73.89\ g/mol} = 57.11\ mol/L$

$$c_{SEI} = \frac{\rho}{M} \approx \frac{1.32 \frac{g}{cm^3}}{102.06 \frac{g}{mol}} = 12.94\ mol/L$$

For Li ethylene carbonate,

$$c_{SEI} = \frac{\rho}{M} \approx \frac{1.07 \frac{g}{cm^3}}{104.08 \frac{g}{mol}} = 10.28\ mol/L$$

For Li-DMC,

$$c_{SEI} = \frac{\rho}{M} \approx \frac{0.98\ g/cm^3}{132.13\ g/mol} = 7.19\ mol/L$$

For Li-DEC,

$$c_{SEI} = \frac{\rho}{M} \approx \frac{1.45\ g/cm^3}{113.05\ g/mol} = 12.83\ mol/L$$

For Li-FEC,

$$c_{SEI} = 20.07\ mol/L$$

$$R = 1.41 \frac{\beta}{\sqrt{\alpha}} t^{1/2} = 1.41 \times \frac{1}{76.3} \times \left(\frac{11.82}{20.07}\right)^{-1/2} \frac{D_{Li^+}^{SEI}}{\sqrt{D_{Sol}^{SEI}}} t^{1/2} = 0.0241 \frac{D_{Li^+}^{SEI}}{\sqrt{D_{Sol}^{SEI}}} t^{0.5}$$

(Supporting Equation 7)

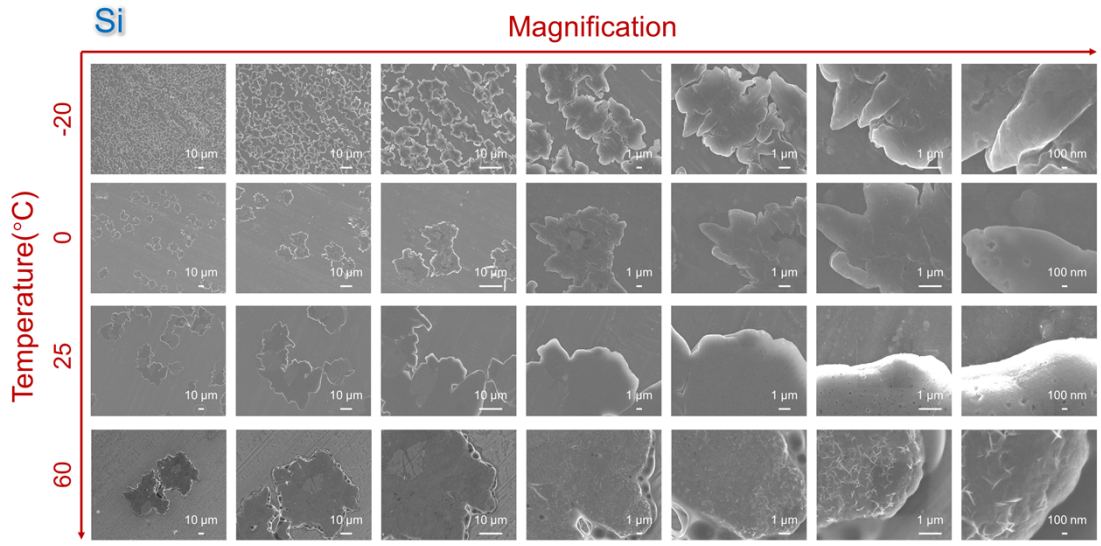

Supporting Figure S26. Temperature effect. SEM images of Li deposits on Si at different temperatures (J=0.025 mA cm^{-2}, Q=0.1 mAh cm^{-2}).

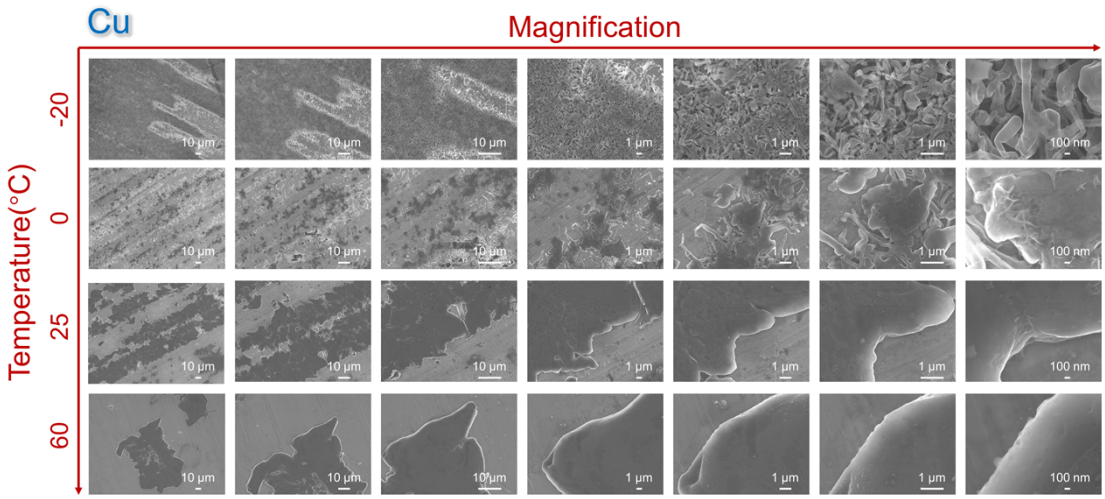

Supporting Figure S27. Temperature effect. SEM images of Li deposits on Cu at different temperatures (J=0.025 mA cm^{-2}, Q=0.1 mAh cm^{-2}).

If current per nuclei(J/N) is surface diffusion limited,

$$\frac{J}{N} \sim C_a \pi r^2 \sim C_a \pi (\sqrt{Dt})^2 = C_a \pi D t = C_a \pi D_0 t e^{-\frac{E_a}{RT}}$$

$$log(\frac{J}{N}) = -\frac{E_a}{R} \cdot \frac{1}{T} + log(C_a \pi D_0 t) \quad \text{(Supporting Equation 8)}$$

Where C_a is concentration of surface adatom, r is diffusion zone radius, D is surface diffusivity, t is time for nucleation.

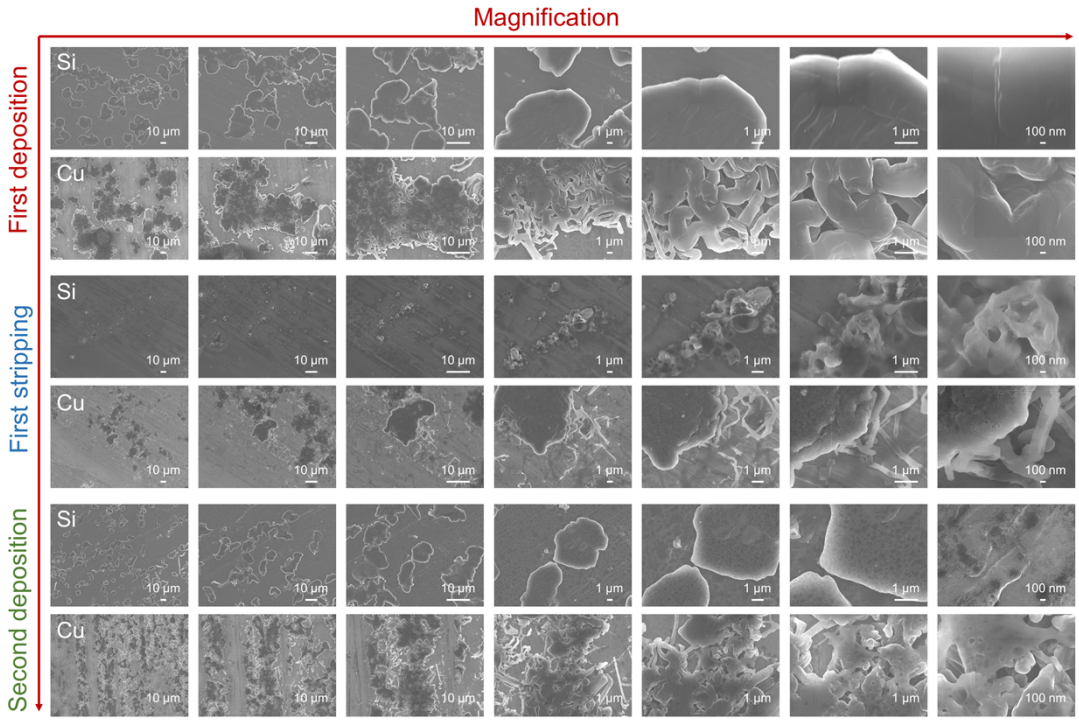

Supporting Figure S28. Reversibility. SEM images after first deposition, first stripping and second deposition (J=0.1 mA cm^{-2}, Q=0.1 mAh cm^{-2}).

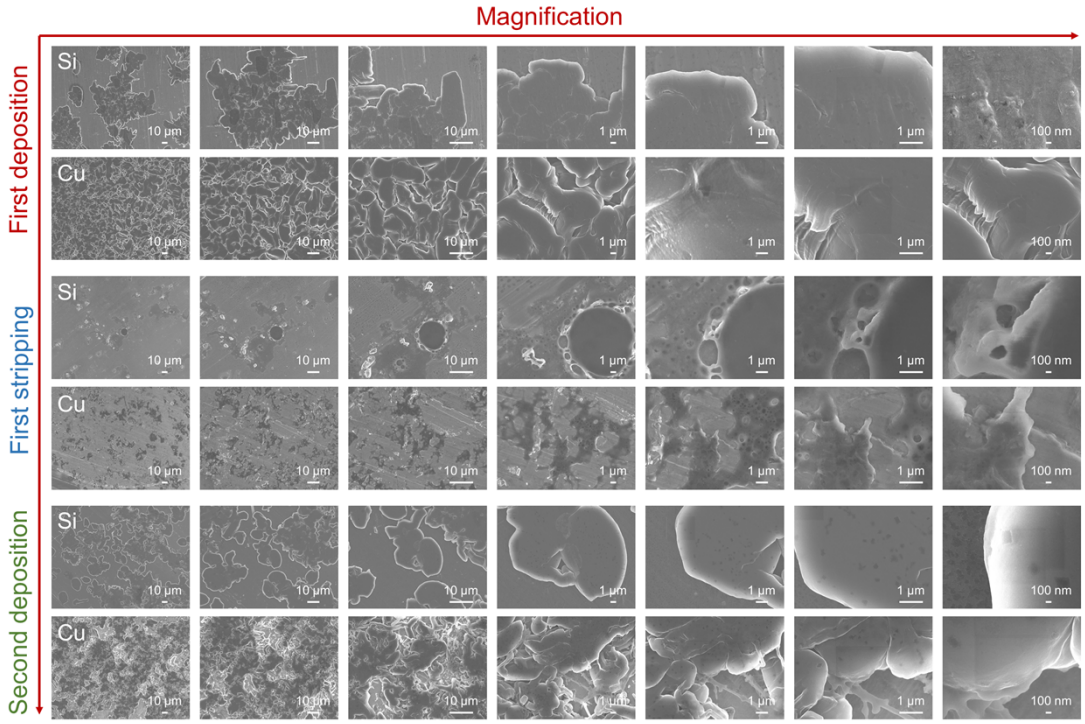

Supporting Figure S29. Reversibility. SEM images after first deposition, first stripping and second deposition (J=0.1 mA cm^{-2}, Q=0.5 mAh cm^{-2}).

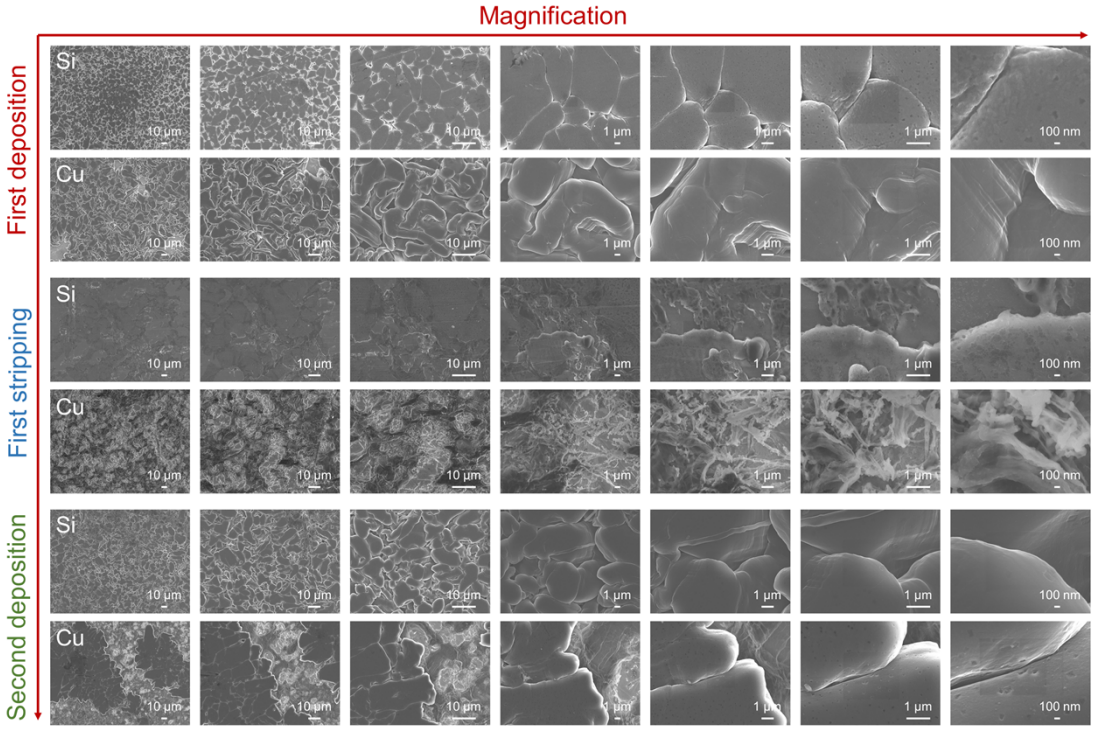

Supporting Figure S30. Reversibility. SEM images after first deposition, first stripping and second deposition (J=0.1 mA cm^{-2}, Q=3 mAh cm^{-2}).

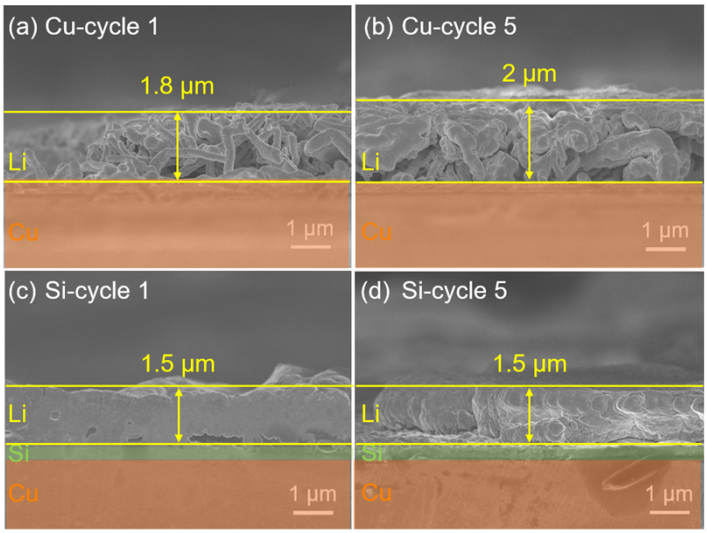

Supporting Figure S31. The cross-sectional SEM images for the deposited Li after 1st cycle and 5th cycle on (a, b) Cu and (c, d) Si. (J=0.1 mA cm^{-2}, Q=0.5 mAh cm^{-2})

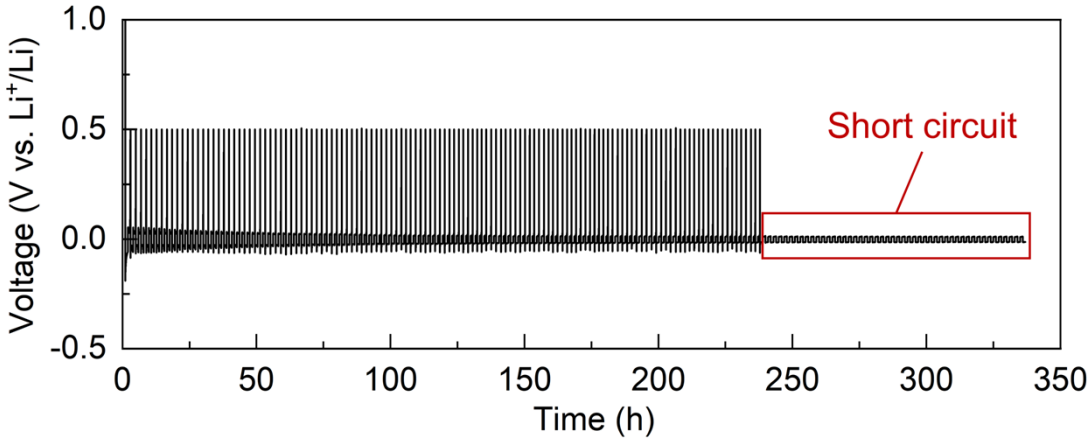

Supporting Figure S32. Reversibility. Cycle curve.

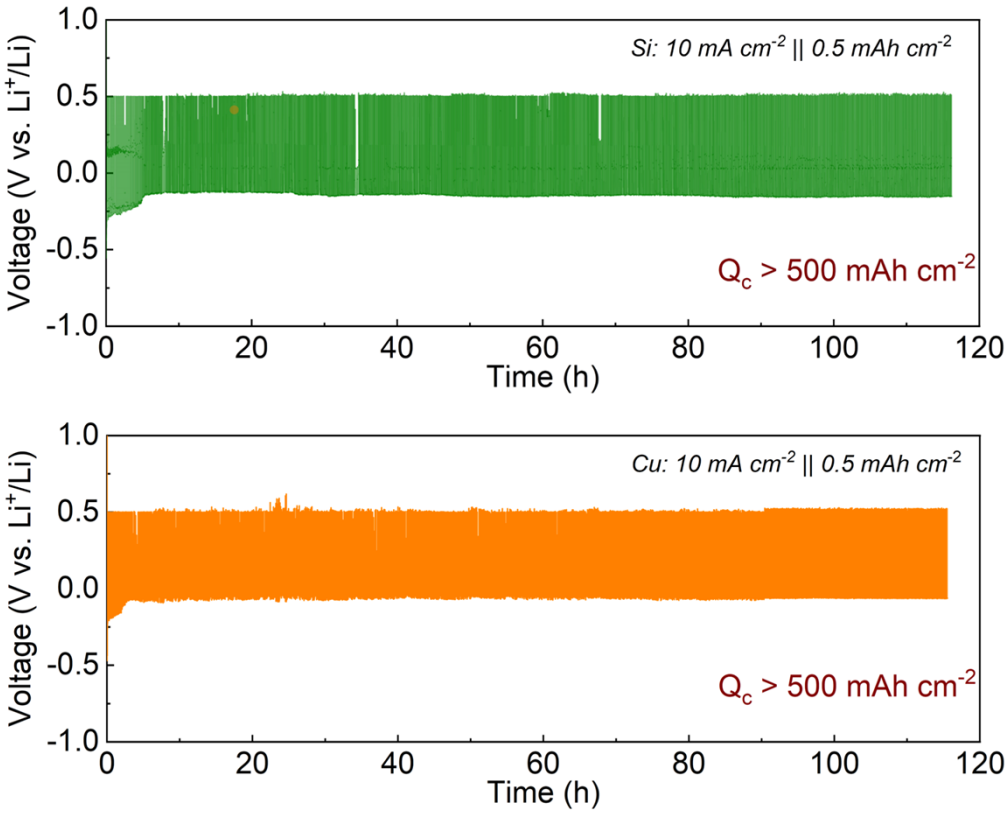

Supporting Figure S33. Reversibility. Cycle curve at 10 mA cm^{-2} for Li|Si and Li|Cu half cells.

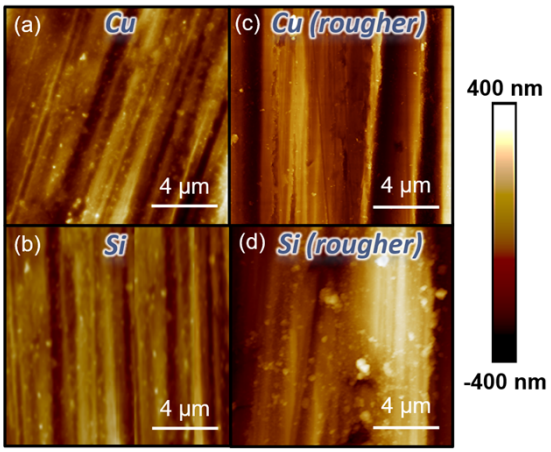

Supporting Figure S34. AFM images of (a) Cu, (b) Si, (c) Cu (rougher), and (d) Si (rougher) substrates.

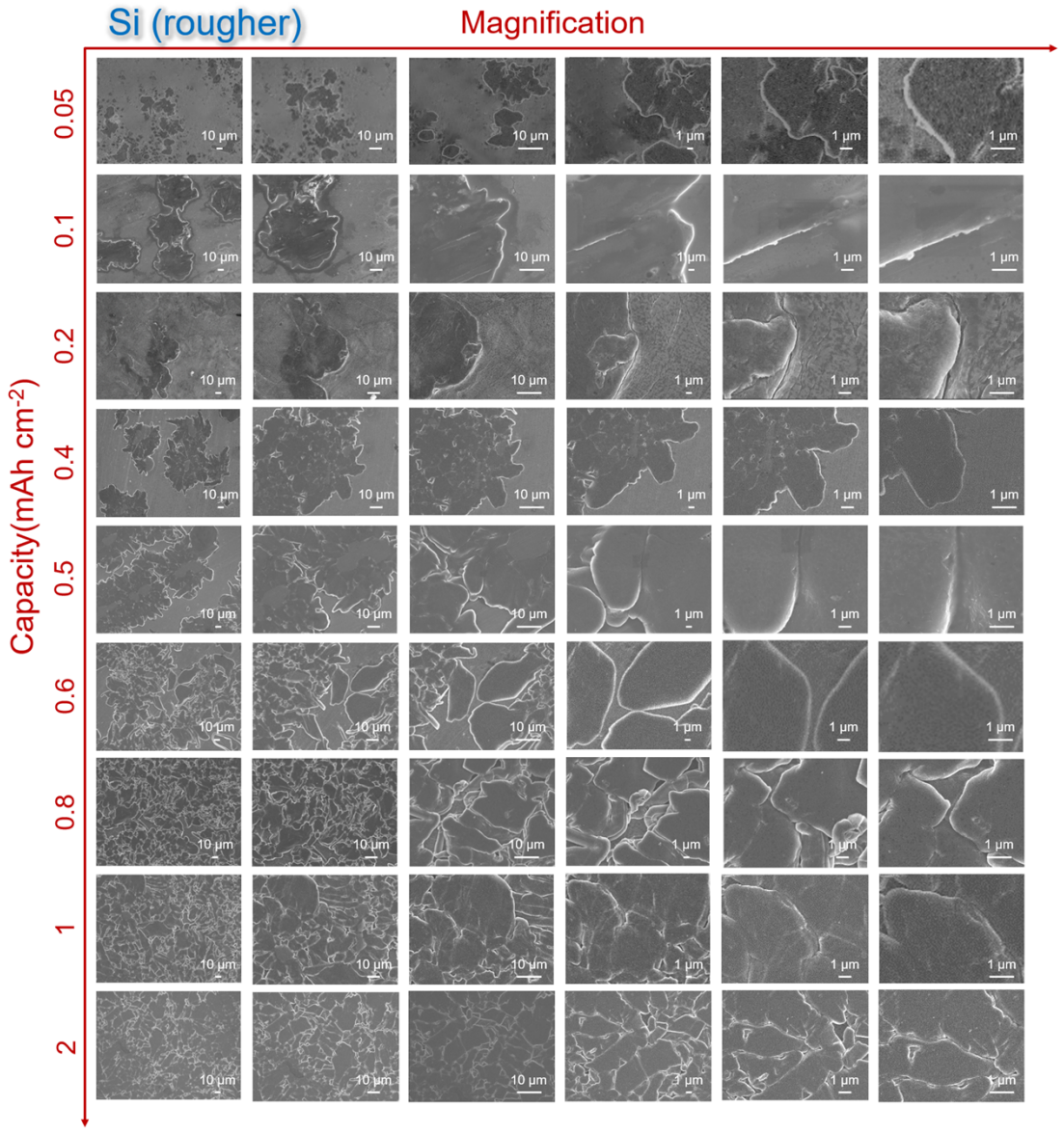

Supporting Figure S35. Li growth on Si (rougher). SEM images of Li deposits at different capacities, J=0.025 mA cm^{-2}.

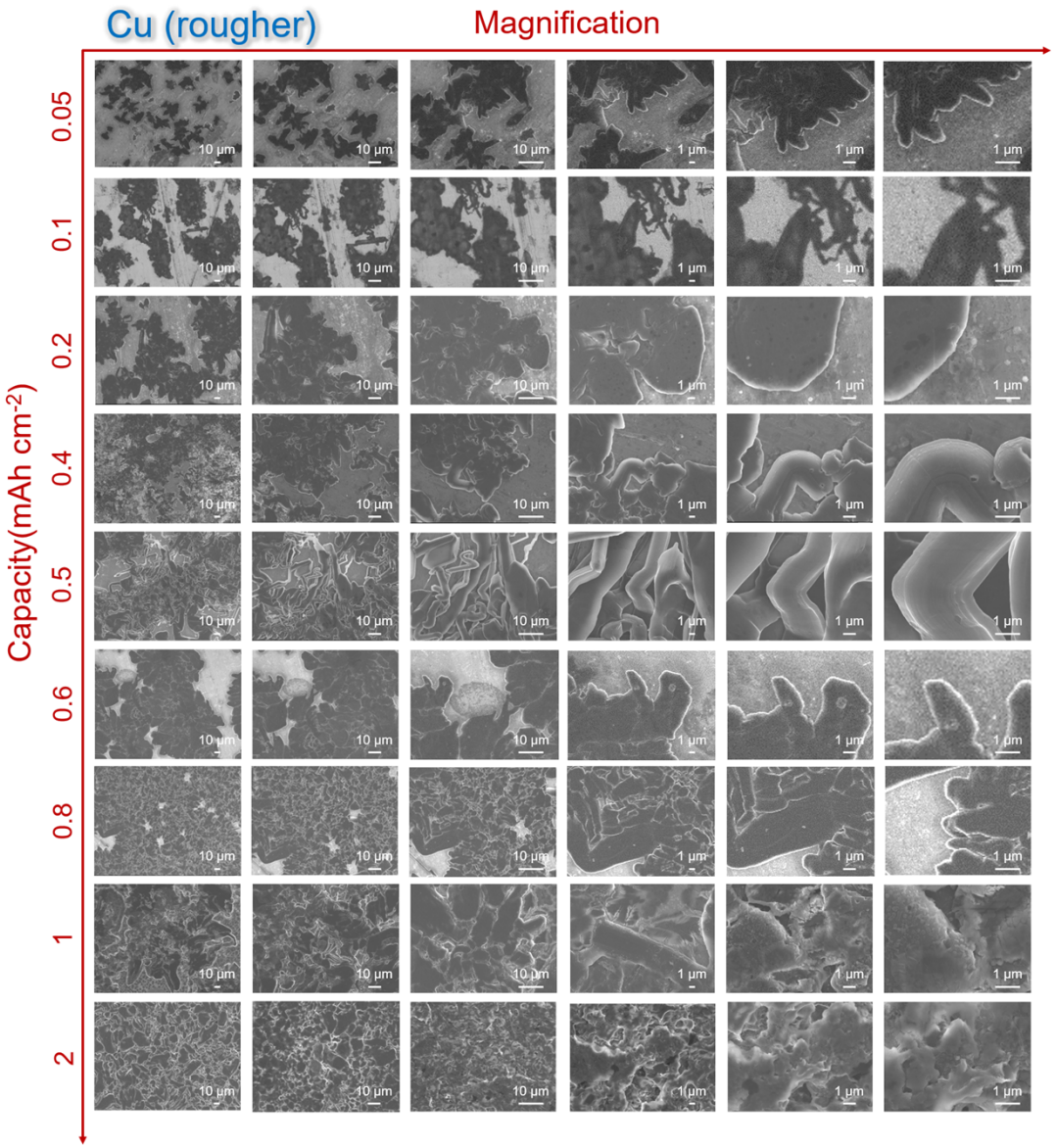

Supporting Figure S36. Li growth on Cu (rougher). SEM images of Li deposits at different capacities, J=0.025 mA cm^{-2}.

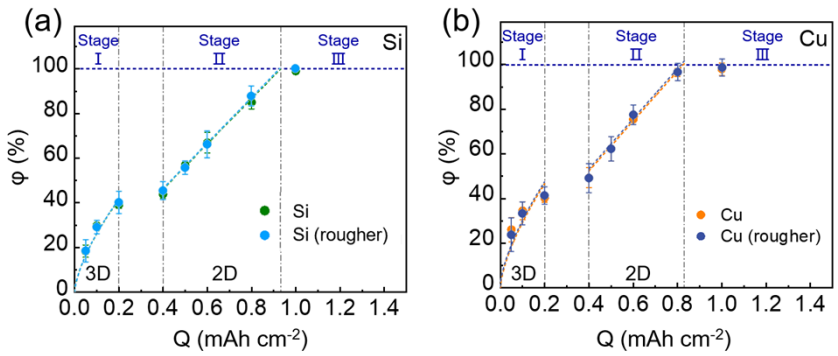

Supporting Figure S37. The quantitative correlations between φ and Q on (a) Si and (b) Cu with different roughness at 0.025 mA cm^{-2}.

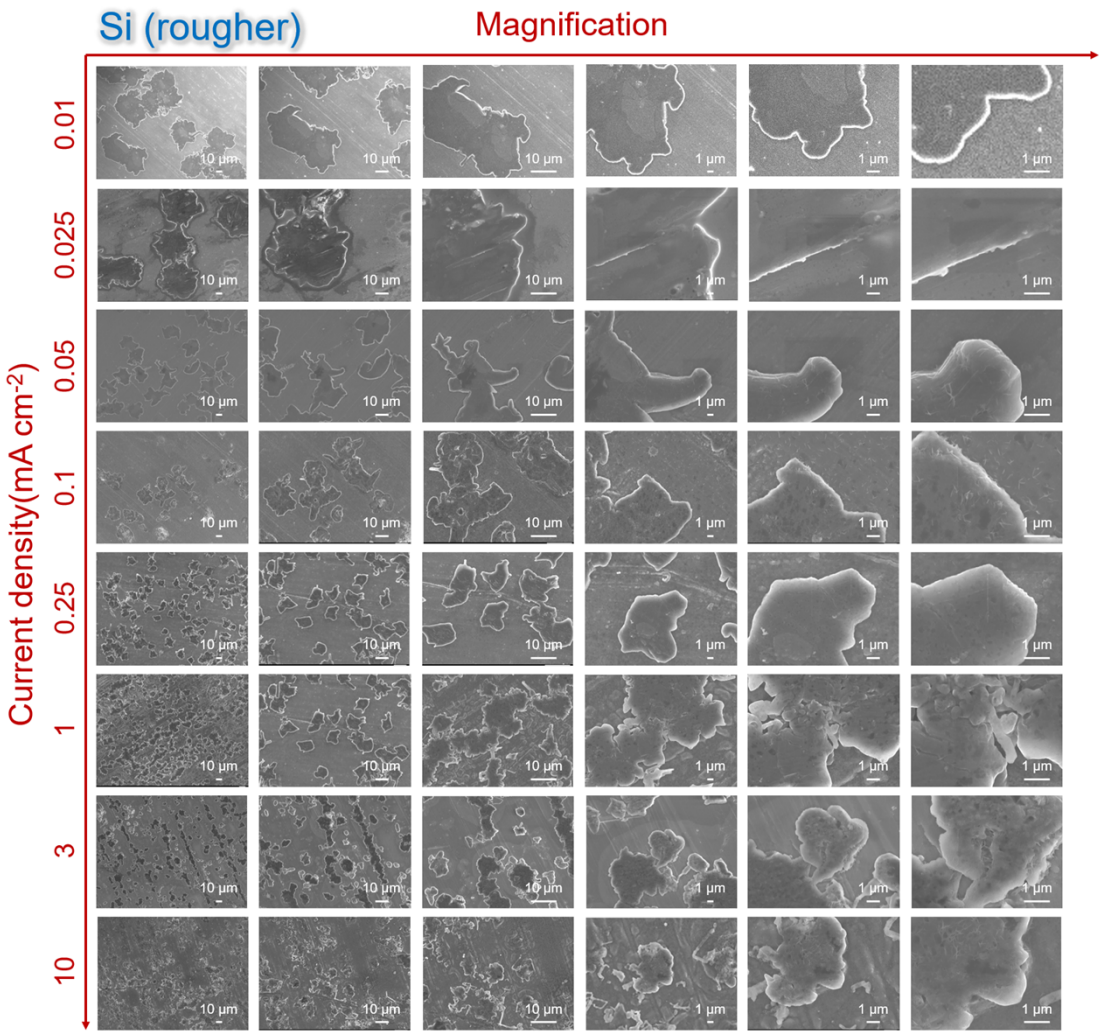

Supporting Figure S38. Li growth on Si (rougher). SEM images of Li deposits at different current densities, Q=0.1 mAh cm^{-2}.

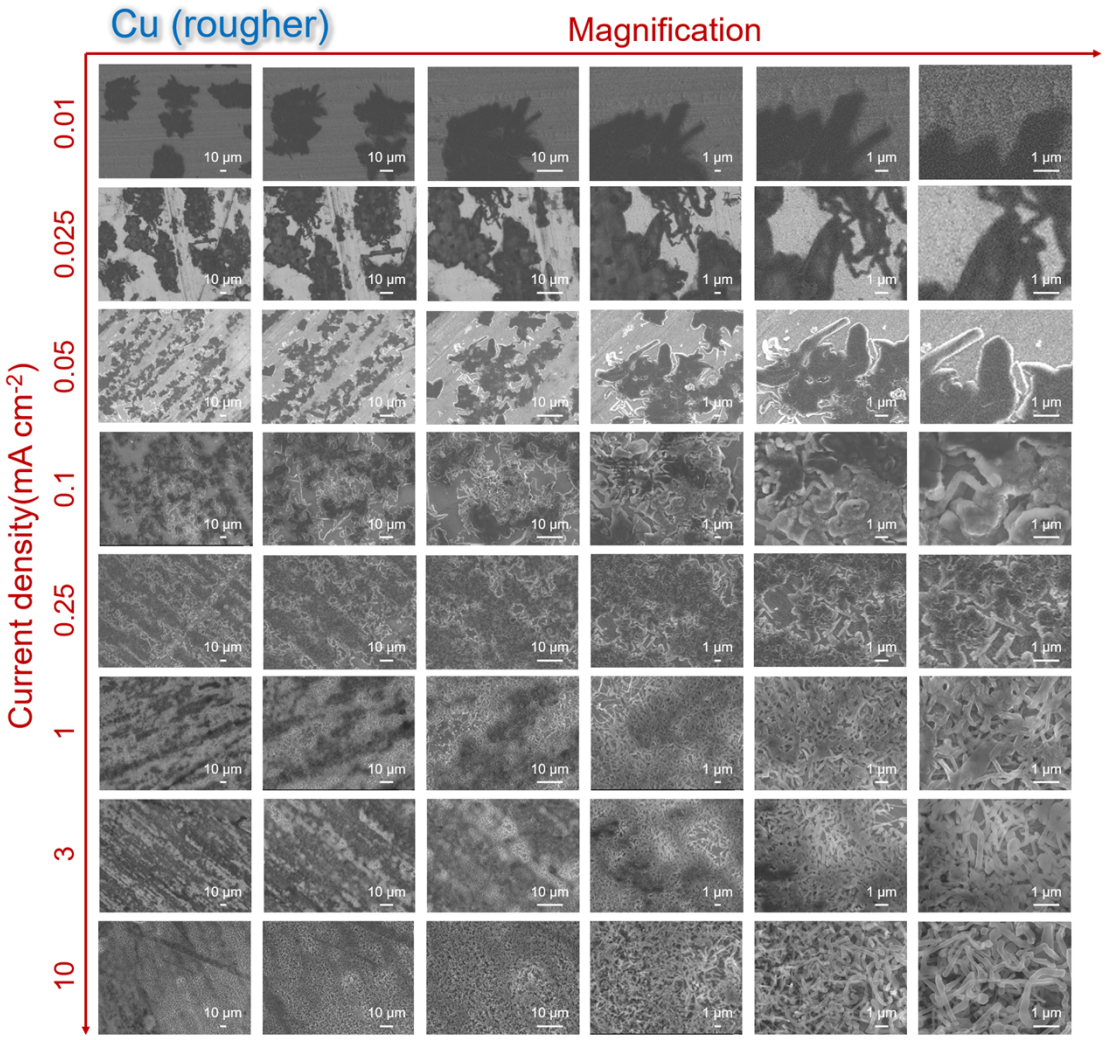

Supporting Figure S39. Li growth on Cu (rougher). SEM images of Li deposits at different current densities, Q=0.1 mAh cm^{-2}.

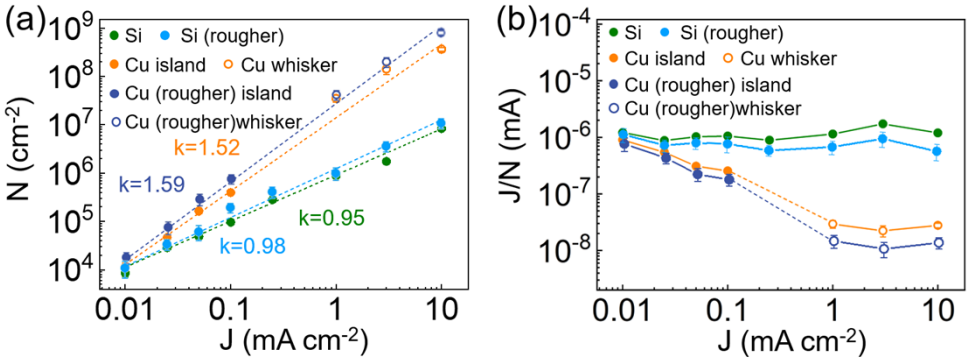

Supporting Figure S40. The quantitative correlations (a) between N and J, (b) between J/N and J on Si and Cu with different roughness using deposition capacity of 0.1 mAh cm^{-2}.

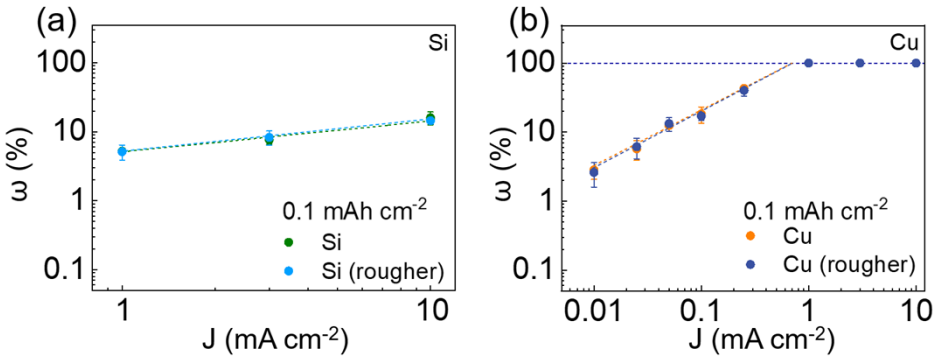

Supporting Figure S41. The quantitative correlations between ω and J on (a) Si and (b) Cu with different roughness using deposition capacity of 0.1 mAh cm^{-2}.

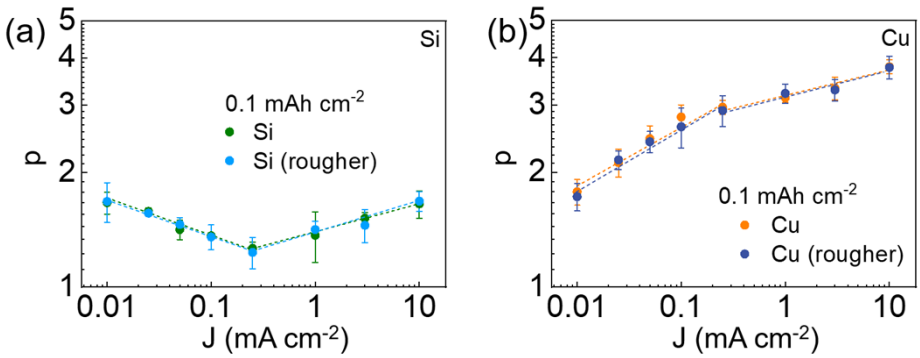

Supporting Figure S42. The quantitative correlations between p and J on (a) Si and (b) Cu with different roughness using deposition capacity of 0.1 mAh cm^{-2}.

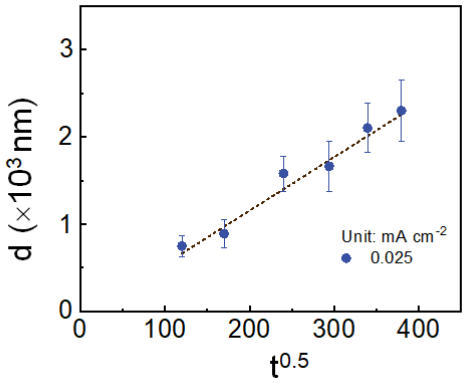

Supporting Figure S43. The quantitative correlation between d and $t^{1/2}$ on Cu (rougher), J=0.025 mA cm^{-2}.

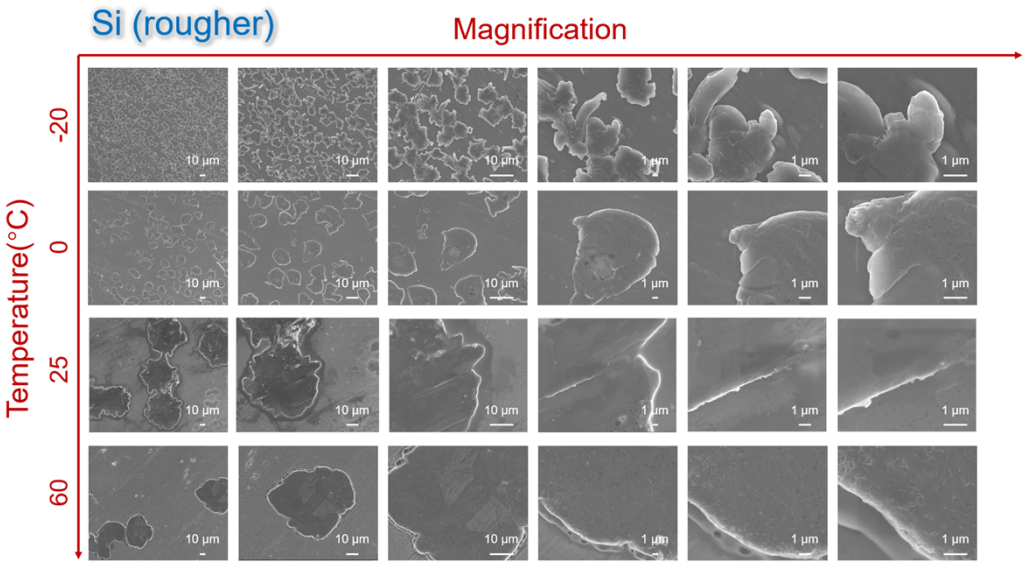

Supporting Figure S44. SEM images of Li deposits on Si (rougher) at different temperatures (J=0.025 mA cm^{-2}, Q=0.1 mAh cm^{-2}).

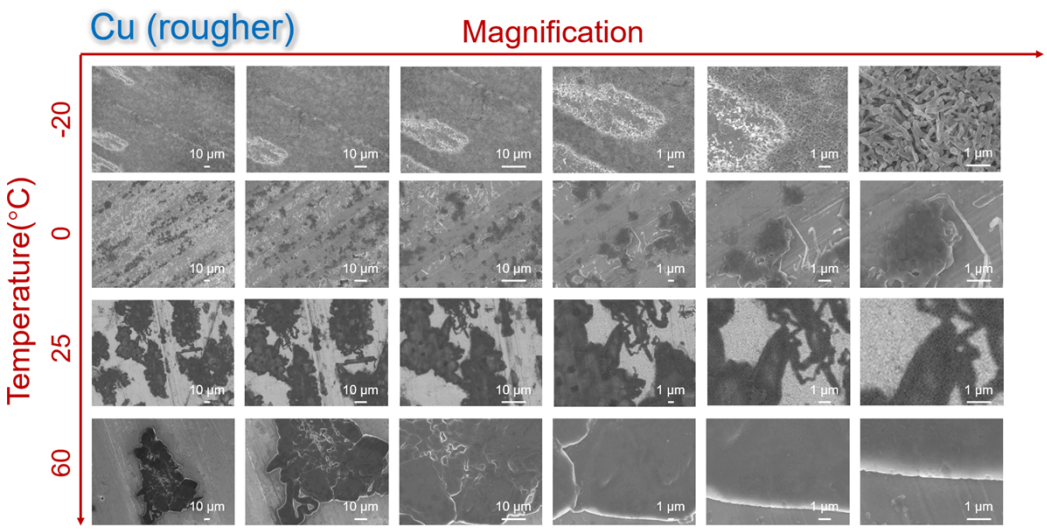

Supporting Figure S45. SEM images of Li deposits on Cu (rougher) at different temperatures (J=0.025 mA cm^{-2}, Q=0.1 mAh cm^{-2}).

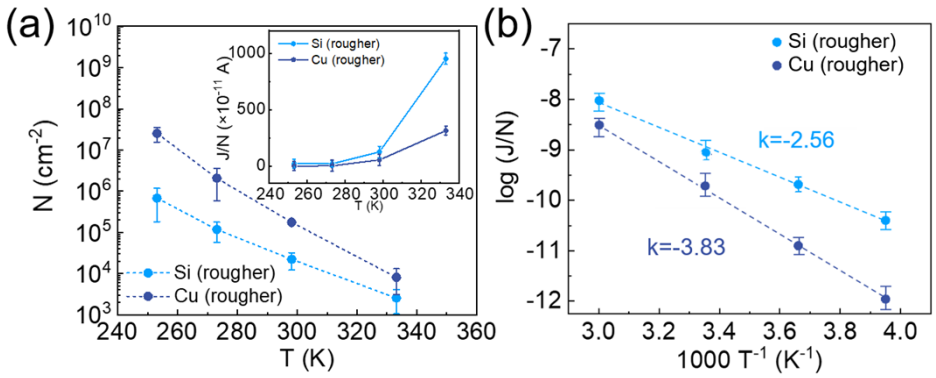

Supporting Figure S46. The quantitative correlations (a) between N and T (inset: J/N vs T), (b) between log (J/N) and T^{-1} on Si (rougher) and Cu (rougher) at different temperatures (J=0.025 mA cm^{-2}, Q=0.1 mAh cm^{-2}).

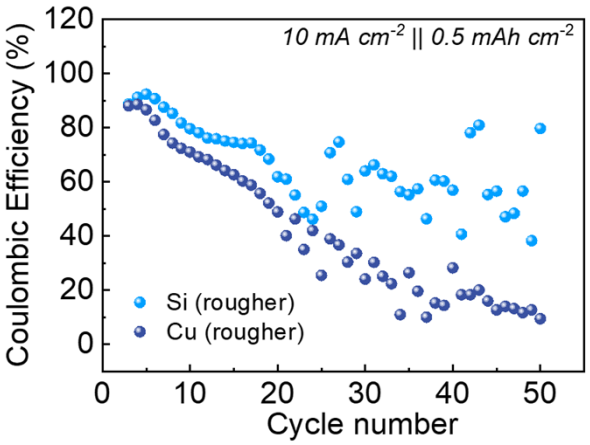

Supporting Figure S47. Reversibility. Columbic efficiency vs cycle number on rougher substrates (J=10 mA cm^{-2}, Q=0.5 mAh cm^{-1}).

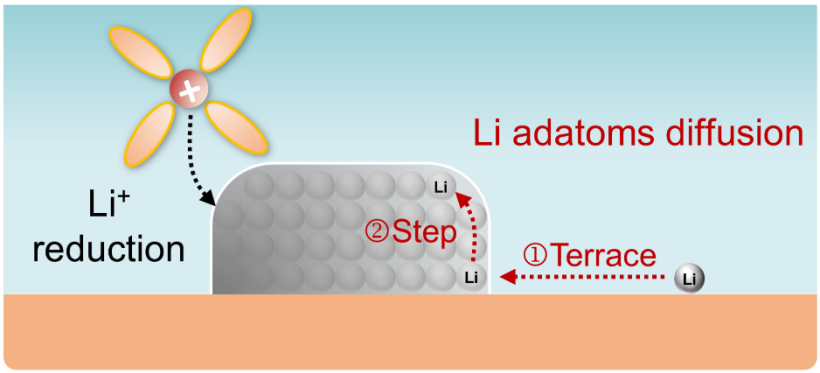

Supporting Figure S48. Two ways for the growth of Li deposits.

Table S1. The simulation results of EIS at different current

Sample	Current density (mA cm^{-2})	ESR (R_1, Ω)	R_f (R_2, Ω)	R_{ct} (R_3, Ω)
Si	0.01	2.648	12.85	147
	0.025	2.03	17.61	109.3
	0.05	2.437	17.18	104.6
	0.1	2.869	21.58	141.8
	0.25	1.929	18.24	118.9
	1	3.239	13.5	173.5
	3	2.232	6.439	124.7
	10	2.916	19.94	53.33
Cu	0.01	1.903	15.94	119.5
	0.025	2.115	21.12	113.2
	0.05	2.152	16.1	180.9
	0.1	1.778	14.26	145.3
	0.25	3.194	14.59	122.6
	1	2.435	30.74	172.1
	3	2.19	33.7	63.4
	10	2.13	7.119	66.12

Linear characteristic at small η_P:

$$J = \omega \eta_P$$

$$\omega = \frac{RT}{J_0 F}$$

$$J_0^{Si} = 0.075\ mA\ cm^{-2}$$

$$J_0^{Cu} = 0.090\ mA\ cm^{-2}$$

Table S2. The simulation results of EIS at different temperature

Sample	Temperature (°C)	ESR (R_1, Ω)	R_f (R_2, Ω)	R_{ct} (R_3, Ω)
Si	-20	6.465	15.44	5783
	0	3.121	12.18	848
	25	2.03	17.61	109.3
	60	2.265	2.774	28.98
Cu	-20	7.061	17.78	5630
	0	4.694	23.89	1061
	25	2.115	21.12	113.2
	60	2.185	2.432	56.22

Parameter definition:

b	The fitting parameter	nm $s^{-0.5}$
d	The diameter of whisker	nm
h	The minimal thickness for full coverage	μm
k_1	The fitting parameter	$mAh^{-2/3}$ $cm^{4/3}$
k_2	The fitting parameter	mAh^{-1} cm^2
l	The length of whisker	nm
m	The fitting parameter	-
n	The formula constant	-
p	The normalized perimeter	-
t	Li deposition time	s
A	The area of deposits	cm^2
$D_{Li^+}^{SEI}$	The diffusivity of Li^+ through SEI	m^2 s^{-1}
D_{Sol}^{SEI}	The diffusivity of solvent through SEI	m^2 s^{-1}
E_s	The activation energy for diffusion of Li adatoms	eV
H	The thickness of Li deposit	μm
J	Current density	mA cm^{-2}
J_w	The critical current for the areal percentage of whisker is 100%	mA cm^{-2}
N	Nucleation density	cm^{-2}
P	The perimeter of deposits	cm
Q	Li deposition capacity	mAh cm^{-2}
Q_c	Total deposition capacity when internal short-circuit occurs	mAh cm^{-2}
Q_h	The minimal capacity for full coverage	mAh cm^{-2}
R_0	The ohmic resistance of the cell	Ω

S	The electrode area	cm^2
T	Temperature	K
V	The volume of 2D deposit	cm^3
SA	The surface area of 2D deposit	cm^2
J/N	Current per nuclei	mA
ε	Porosity	%
η_n	Nucleation overpotential	mV
η_p	Plating overpotential	mV
η_{ohm}	Ohmic overpotential	mV
φ	The coverage of the substrate by the deposits	%
ω	The areal percentage of whisker	%

Notes and references:

1 S. Plimpton, *J. Comput. Phys.*, 1995, **117**, 1-19.

2 A. Stukowski, *Model. Simul. Mater. Sc.*, 2009, **18**, 015012.

3 W. G. Hoover, *Phys. Rev. A*, 1985, **31**, 1695-1697.

4 M. I. Baskes, *Phys. Rev. B*, 1992, **46**, 2727-2742.

5 J. Tersoff, *Phys. Rev. B*, 1988, **37**, 6991-7000.

6 C. Fang, B. Lu, G. Pawar, M. Zhang, D. Cheng, S. Chen, M. Ceja, J.-M. Doux, H. Musrock, M. Cai, B. Liaw and Y. S. Meng, *Nat. Energy*, 2021, **6**, 987-994.

7 V. Ponce, D. E. Galvez-Aranda and J. M. Seminario, *J. Phys. Chem. C*, 2017, **121**, 12959-12971.

8 A. K. Rappe, C. J. Casewit, K. S. Colwell, W. A. Goddard and W. M. Skiff, *J. Am. Chem. Soc.*, 1992, **114**, 10024-10035.